 doi:10.20944/preprints202108.0578.v1

Rare Earth Elements Enhanced the Oxidation Resistance of Mo-Si-Based Alloys for High Temperature Application: A Review

Laihao Yu[a], Yingyi Zhang[a,*], Tao Fu[a], Jie Wang[a], Kunkun Cui[a], Fuqiang Shen[a]

[a] School of Metallurgical Engineering, Anhui University of Technology, Maanshan 243002, Anhui Province, China

* Correspondence: author: Yingyi Zhang (Y.Y. Zhang) E-mail : zhangyingyi@cqu.edu.cn (Y.Y. Zhang), Tel.: +86 17375076451

Abstract: Traditional refractory materials such as nickel-based superalloys have been gradually unable to meet the performance requirements of advanced materials. The Mo-Si-based alloy, as a new type of high temperature structural material, has entered the vision of researchers due to its charming high temperature performance characteristics. However, its easy oxidation and even "pesting oxidation" at medium temperatures limit its further applications. In order to solve this problem, researchers have conducted large numbers of experiments and made breakthrough achievements. Based on these research results, the effects of rare earth elements like La, Hf, Ce and Y on the microstructure and oxidation behavior of Mo-Si-based alloys were systematically reviewed in the current work. Meanwhile, this paper also provided an analysis about the strengthening mechanism of rare earth elements on the oxidation behavior for Mo-Si-based alloys after discussing the oxidation process. Furthermore, the research focus about the oxidation protection of Mo-Si-based alloys in the future was prospected to expand the application field.

Keywords: Mo-Si-based alloys; Alloying; Rare earth elements; Oxidation behavior; Mechanism

1. Introduction

As the world population increases, the problem of global resource shortage has become increasingly prominent. It is well known that in addition to waste recycling, improving energy utilization and exploring new energy are effective methods to solve resource problems, and are also the main trend of future scientific and technological development [1-3]. Nowadays, the development of new energy is overwhelming. As a new high temperature structural material, the Mo-Si-based alloy is expected to replace the nickel-based alloy and play an important role in turbine engine and industrial furnace components [4-7].

A large number of studies have pointed out that Mo-Si-based alloys have outstanding high temperature performance characteristics, such as moderate density, strong electrical and thermal conductivity, ultra-high melting point, high thermal impact resistance, etc., which has been widely used in various industries [8-11]. However, these alloys also have some inherent defects that limit their generalization as structural materials

Preprints (www.preprints.org) | NOT PEER-REVIEWED | Posted: 31 August 2021 doi:10.20944/preprints202108.0578.v1

[12-14]. For example, $MoSi_2$-based alloys exhibit low room temperature fracture toughness, poor high temperature creep resistance, and catastrophic oxidation at 400 ℃ to 800 ℃. Although Mo_5Si_3-based alloys have relatively strong creep resistance, they generally present accelerated oxidation or "pesting oxidation" phenomenon below 1000 ℃, which is a thorny problem [15-19]. To overcome these shortcomings, relevant researchers have been working hard since the end of the 20th century [20-25]. Fortunately, people finally succeeded in improving the properties of alloy through material designs [26-29], preparation techniques [30-34] or surface modification methods [35-38]. Among them, doping second phases such as W, Nb, ZrO_2, La_2O_3, Al_2O_3, Cr_2O_3 in material designs to strengthen the performance of substrate is generally regarded as an important measure [39-41].

There is no doubt that in some refractory metal materials like niobium-based, molybdenum-based and tungsten-based materials, adding active elements may significantly improve the mechanical properties [42-44]. Rare earth or its oxides, as a kind of active element, have received particular attentions and widespread applications [45-48]. In recent years, researchers have made great breakthroughs in studying rare earth elements to enhance the mechanical properties of metal materials. However, so far, there are few reports on the oxidation behavior of Mo-Si-based alloy doped with rare earth elements. Therefore, this paper comprehensively and systematically reviewed the actions of rare earth elements such as La, Hf, Ce and Y on the antioxidant properties of Mo-Si-based alloys, especially the Mo-Si-B system, and summarized the relevant strengthening mechanisms.

2. Effects of rare earth elements on oxidation behavior of Mo-Si-based alloys

It's well known that the increase of oxide layer thickness is primarily caused by the internal diffusion of O_2 [49-52], and studies have shown that alloying with active elements can effectively reduce the internal diffusion rate of O_2 [53-55]. For example, appropriate adding rare earth elements, on the one hand, can separate oxygen atoms at the metal-oxide interfaces and oxide scale grain boundaries and react with O_2, thus hindering the diffusion of O_2 [56-59]. On the other hand, it can optimize the oxide scale microstructure and improve the scale adhesion [60-63]. Therefore, alloying with rare earth elements is of great significance to enhance the antioxidant properties. The influences of adding rare earth elements like La, Hf, Ce and Y on the oxidation behavior of Mo-Si-based alloys will be reviewed in detail below.

2.1 Effects of rare earth elements on oxidation behavior of Mo-Si-B alloys

Among all kinds of Mo-Si-based alloys, the most widely studied are Mo-Si-B alloys because of their excellent characteristics[64-70]. Therefore, it's very necessary to explore the effects of rare earth elements on

Preprints (www.preprints.org) | NOT PEER-REVIEWED | Posted: 31 August 2021 doi:10.20944/preprints202108.0578.v1

oxidation behavior of Mo-Si-B alloys.

2.1.1 Effects of La element addition

Compared with pure Mo-Si alloys, adding La element can significantly optimize the microstructure of these alloys by the means of reducing the grain size and making the intermetallic particles disperse more evenly, thus improving the fracture toughness, bending and compressive strength significantly [71-74]. Based on the existing studies of Mo-12Si-8.5B alloy (at.%) [75-79], we further analyzed the actions of doping La or La_2O_3 second phase on the oxidation behavior.

Zhang et al. [80] prepared Mo-12Si-8.5B (at.%, abbreviated as MSB) samples added with different contents of La_2O_3 through arc-melted and spark plasma sintered methods, and the specific contents were presented in Table 1. Fig. 1 (a) gives the XRD patterns of MSB+xLa_2O_3 samples (x=0, 0.3, 0.6, 1.2 wt.%). It can be seen that all the samples consist of Mo_5SiB_2, Mo_3Si and α-Mo three phases, which is consistent with the phase diagram of isothermal Mo-Si-B composites [76]. At the same time, it also reveals that even if La_2O_3 is added will not affect the phase composition of samples. Figs. 1 (b-e) are micrographs of the four samples prepared, where the white regions are α-Mo phase, and the black regions are Mo_5SiB_2/Mo_3Si phases dispersed in the α-Mo matrix. It can also be found from micrographs that the grain size of α-Mo and Mo_5SiB_2/Mo_3Si will be reduced after adding La_2O_3, in which the α-Mo size change is more pronounced, whereas the decrease of each phase size is not sensitive to the La_2O_3 mass fraction. Moreover, the distribution of Mo_5SiB_2/Mo_3Si phases is more uniform after doping La_2O_3. This is because parts of La_2O_3 can be used as nucleation sites, which leads to the increase of nucleation density. On the other hand, La_2O_3 particles play a "pinning" role on the α-Mo boundary to inhibit its grains growth. The results in Table 1 further reveal the effect of La_2O_3 on grain size.

Table 1. The La_2O_3 mass fractions and grain sizes of various samples studied. Reproduced with permission [80]. Copyright 2011 Elsevier.

Materials	MSB	MSB + 0.3	MSB + 0.6	MSB + 1.2
Mass fraction of La_2O_3 (wt.%)	0	0.3	0.6	1.2
Grain sizes of α-Mo (μm)	19.78	10.88	9.56	9.46
Grain sizes of Mo_3Si/Mo_5SiB_2 (μm)	3.04	2.46	2.55	2.17

Preprints (www.preprints.org) | NOT PEER-REVIEWED | Posted: 31 August 2021 doi:10.20944/preprints202108.0578.v1

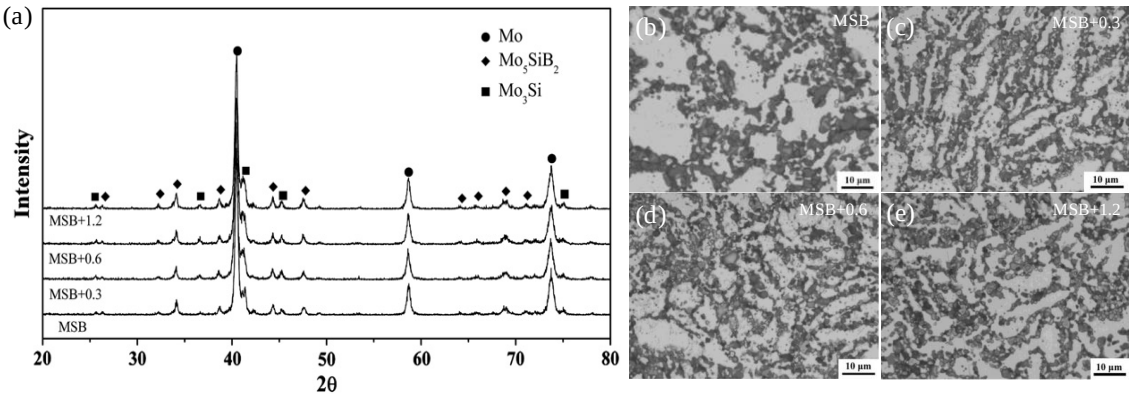

Fig. 1. XRD patterns (a) and microstructure images (b-e) of MSB+xLa_2O_3 samples (x=0, 0.3, 0.6, 1.2 wt.%) before oxidation. Reproduced with permission [80]. Copyright 2011 Elsevier.

Weight variation curves for different mass fraction La_2O_3-doped MSB samples after oxidation at 800 ℃ are shown in Fig. 2 (a). The results point out that the mass loss of alloy can be significantly reduced after adding La_2O_3, where MSB+0.6 sample exhibits the least mass loss during transient oxidation stage. It is due to the fact that La_2O_3-doped MSB samples present a finer grain size, which makes it faster to form a protective borosilicate scale to prevent further volatilization of MoO_3. The role of grain refinement has also been reported elsewhere [81-87]. Again, La_2O_3 in the alloy can decrease the grain boundary transport rate, leading to the reduction of weight loss rate. To determine the impact of La_2O_3 on the oxidation behavior, Zhang et al. [80] further studied the cross-sectional structure of MSB+0.6 sample oxidized at 800 ℃. It has been noticed from Fig. 2 (d) that the cross section of this sample is composed of oxidation scale, interlayer and substrate. Among them, the top layer is the dense B_2O_3-SiO_2 scale and the interlayer comprised with MoO_2, which is confirmed by XRD analysis and the content of each element (i.e. Mo, Si, B, O). Furthermore, compared with MSB sample, the intensity and peaks of B_2O_3 and SiO_2 of MSB+0.6 sample are raised visibly (Fig. 2 (b)), indicating that the antioxidant capacity of MSB+0.6 sample is enhanced. Burk [88, 89] and Jéhanno [90] et al. also reported similar results.

In addition, Majumdar et al. [59, 60] also investigated the oxidizability of Mo-9Si-8B (at.%) sample doped with 2at.% La at 750-1400℃. It is established that the La-doped sample exhibits relatively good antioxidant capability below 1000 ℃, which is the result of stable lanthanum oxides like $3La_2O_3 \cdot MoO_3$, La_2O_3 and $La_2O_3 \cdot 3MoO_3$ produced at the oxidation scale to inhibit the formation and volatilization of MoO_3. However, when the temperature exceeded 1000 ℃, the addition of La might adversely affect the sample oxidation properties. Fig. 2 (c) displays the weight change curves of La-doped and undoped samples at 1300 ℃, it can be discovered that the weight loss of La-doped sample is significantly higher than that of undoped sample.

Preprints (www.preprints.org) | NOT PEER-REVIEWED | Posted: 31 August 2021 doi:10.20944/preprints202108.0578.v1

This is because adding La makes the sample cross section present a loose and porous oxide layer structure when oxidized at 1200 ℃ (Fig. 2 (e)). Meanwhile, as oxidation temperature rises to 1300 ℃, a large number of cracks and holes are observed on the sample surface (Fig. 2 (f)), which provides a pathway for O_2 internal diffusion and MoO_3 volatilization. In contrast, even if undoped sample is oxidized at 1300 ℃ for 72 h, a continuous and compact oxidation scale can be still observed in its cross section (Fig. 2 (g)) [88]. Thus, undoped sample has better antioxidant properties in high-temperature environments.

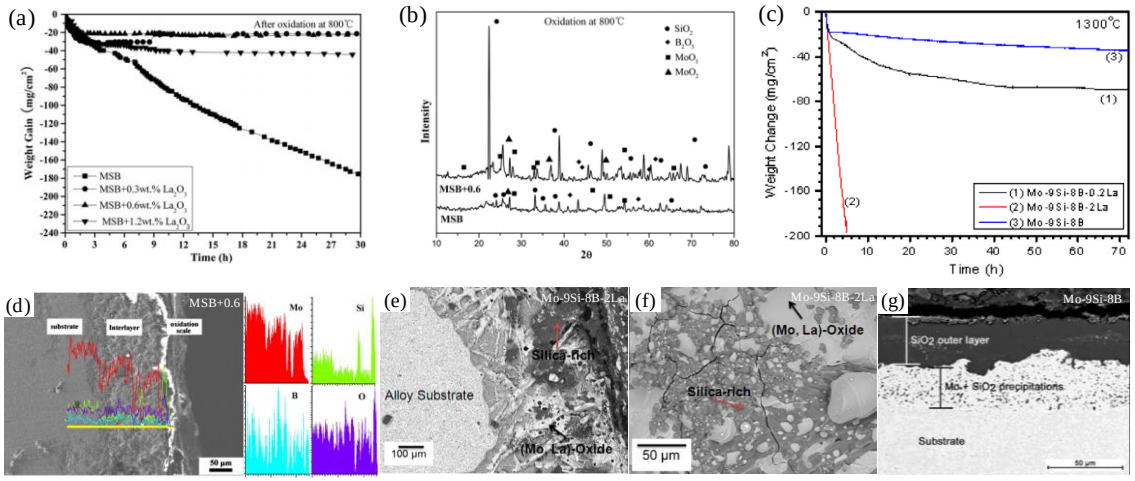

Fig. 2. Weight change curves of various samples oxidized at defferent temperatures (a, c); Surface and cross-sectional SEM/BSE images of various samples oxidized at different conditions: 800 ℃ (d) with corresponding surface XRD analysis results (b), 1200 ℃ for 2 h (e), 1300 ℃ for 23 h (f), 1300 ℃ for 72 h (g). (a, b, d), (c, e, f) and (g) reproduced with permissions [80], [60] and [88], respectively. Copyright 2011 Elsevier, 2014 Elsevier and 2009 Taylor & Francis.

2.1.2 Effects of Hf element addition

Extensive experiments have reported that adding Hf/HfB_2 to Mo-Si-B composites can clearly improve their performance features, such as high temperature strength, high temperature stability, creep resistance, fracture toughness, etc. [91-95]. Potanin et al. [96] discussed the oxidation behavior of MoB-HfB_2-$MoSi_2$ composites at 1200 ℃ in detail. The composition of each alloy is illustrated in Table 2, where the difference between $X34_2$ and $X34_1$ samples is that the former presents two-level structure (TLS), while the latter presents single-level structure (SLS). The microstructures of studied samples is depicted in Figs. 3 (a-c), on the whole, the three samples all contain MoB and $MoSi_2$ phases. The difference is that $X34_1$ and $X34_2$ samples also have additional $HfSiO_4$ and HfB_2 phases and their grain sizes are finer than that of X0 sample. Fig. 4 gives the oxidation kinetics curves of the three samples, it can been observed that the weight increases of $X34_1$ and $X34_2$

Preprints (www.preprints.org) | NOT PEER-REVIEWED | Posted: 31 August 2021 doi:10.20944/preprints202108.0578.v1

samples are more obvious because adding HfB_2 can make the samples generate $HfSiO_4$ (6.97 g/cm^3) and HfO_2 (9.68 g/cm^3), whose specific weights are greater than SiO_2 (2.36 g/cm^3) [97]. By the way, the weight gain of $X34_1$ sample is smaller than that of $X34_2$ sample owing to the fact that $X34_2$ sample presents special arrangement and finer grain size.

Figs. 3 (d-i) show the cross-sectional structure of X0, $X34_1$ and $X34_2$ samples after oxidation at 1200 ℃ for 30 h. It has been noticed that the $X34_1$ and $X34_2$ samples do produce $Si_{x-1}Hf_xO_2/HfSiO_4$ phases during the oxidation process, which is consistent with the above analysis results. Meantime, two-layered oxide films are formed on the surface of all samples, whereas there are great differences in the oxide-film composition and structure. In other words, the X0 sample oxide scale containing SiO_2 layer (top layer) and Mo_5Si_3 layer (bottom layer), the $X34_1$ sample oxide scale consists of $Si_{x-1}Hf_xO_2$-doped amorphous SiO_2 layer (upper layer) and crystalline α-SiO_2 layer (lower layer), while the $X34_2$ sample oxide scale is comprised with crystalline α-SiO_2 layer (outermost layer) and $HfSiO_4$ layer (interlayer). Among them, the formation of amorphous SiO_2 in $X34_1$ sample is due to the dissolution of hafnium. Furthermore, $Si_{x-1}Hf_xO_2$ is generated because hafnium and silicon are equivalent elements leading to the incorporation of hafnium into the lattice of silica, as shown in Fig. 5. It is worth noting that the $X34_2$ sample oxide scale exhibits denser structure is caused by the existence of high wetting angle makes SiO_2-B_2O_3 melt can shrink $HfSiO_4$ particles together, resulting in the formation of smooth and compact oxide films [98].

To summarize, addition of HfB_2 to X0 sample can produce $HfSiO_4/Si_{x-1}Hf_xO_2$ particles dispersed in oxide film, and even form an $HfSiO_4$ interlayer. It has been proved that the $HfSiO_4$ and $ZrSiO_4$ particles have similar effects. On the one hand, they can promote the healing of cracks and holes in borosilicate scale [99, 100], on the other hand, they can both act as barriers and $HfSiO_4$ particles can also increase the crystallization temperature of amorphous scale [101]. Therefore, adding HfB_2 can enhance the alloy antioxidant effects. The research results of Sciti et al. also confirmed this conclusion [97].

Table 2. The elemental composition of various samples. Reproduced with permission [96]. Copyright 2019 Elsevier.

Samples	Composition (at.%)			
	Mo	Hf	Si	B
X0	35.0	-	60.0	5.0
$X34_1$	23.2	11.3	39.7	25.8
$X34_2$				

Preprints (www.preprints.org) | NOT PEER-REVIEWED | Posted: 31 August 2021 doi:10.20944/preprints202108.0578.v1

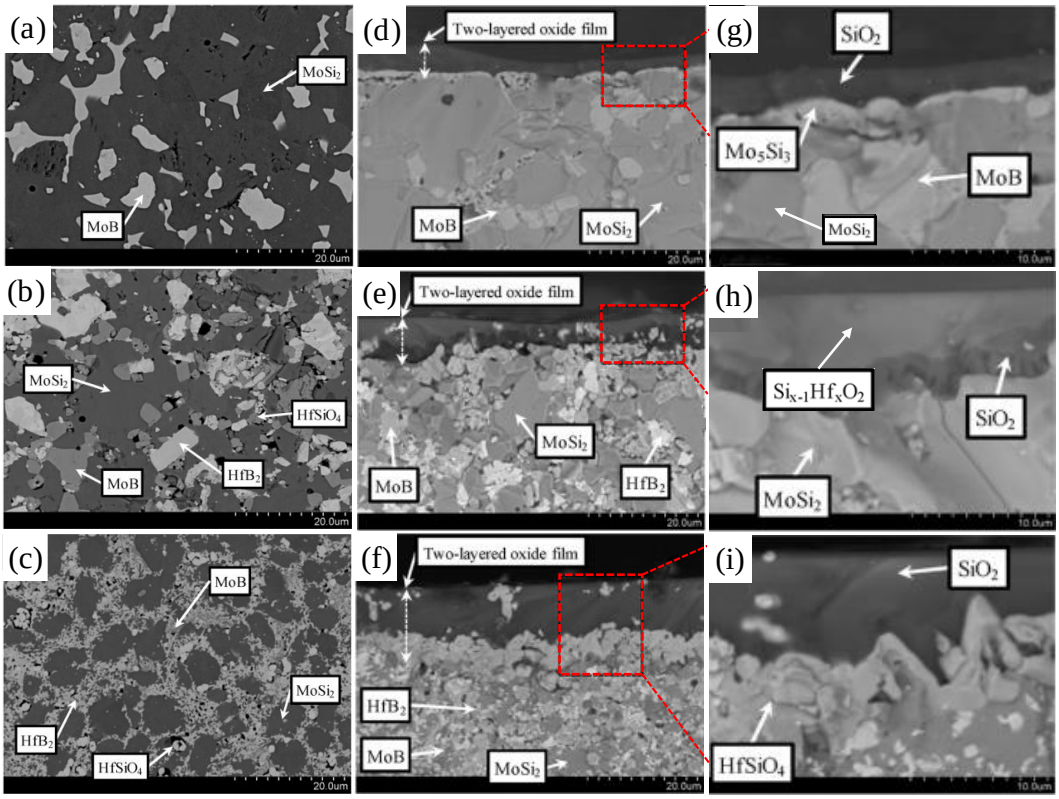

Fig. 3. Microstructure of various samples: (a) X0, (b) $X34_1$ and (c) $X34_2$; Cross-sectional SEM images of samples after oxidation at 1200 ℃ for 30 h: (d, g) X0, (e, h) $X34_1$ and (f, i) $X34_2$. Reproduced with permission [96]. Copyright 2019 Elsevier.

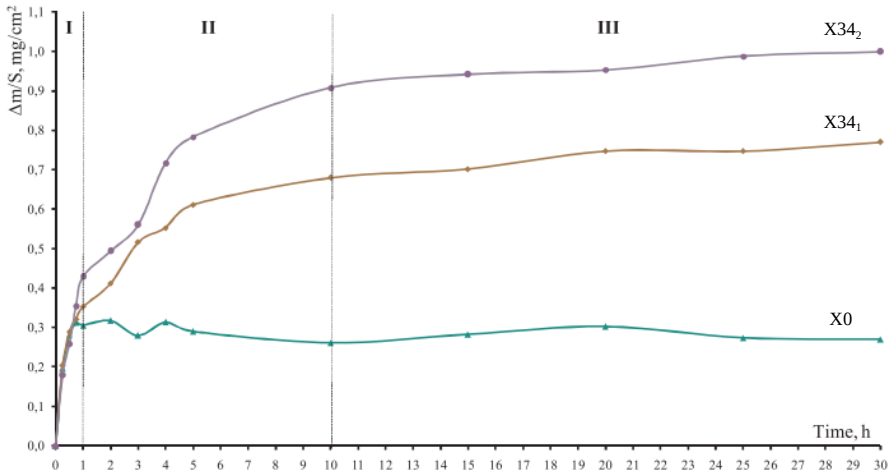

Fig. 4. Kinetic curves of the samples oxidized at 1200 ℃. Reproduced with permission [96]. Copyright 2019 Elsevier.

Preprints (www.preprints.org) | NOT PEER-REVIEWED | Posted: 31 August 2021 doi:10.20944/preprints202108.0578.v1

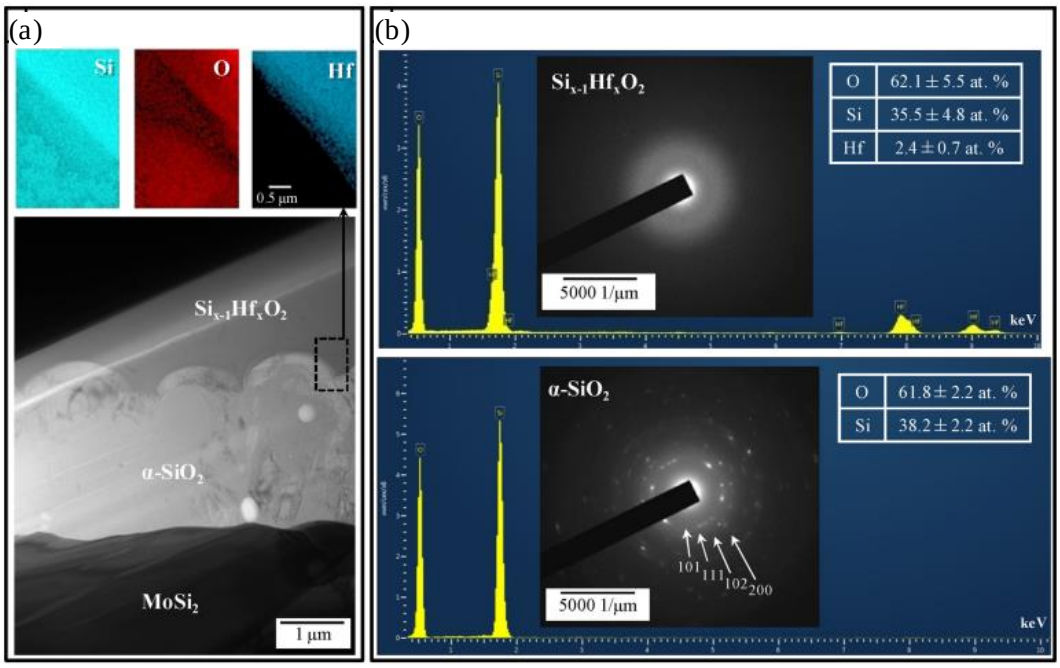

Fig. 5. (a) TEM micrograph of the oxidized $X34_1$ sample; (b) EDS and diffraction patterns of the oxide scale. Reproduced with permission [96]. Copyright 2019 Elsevier.

2.1.3 Effects of Ce element addition

Actions of Ce on oxidation performance of Mo-Si-B alloys have been investigated deeply. Das et al. [102, 103] performed isothermal oxidation experiments about Mo-14Si-10B and Mo-13.98Si-9.98B-0.16Ce alloys (at.%, abbreviated as MSB_1 and MSBCe, respectively) synthesized by arc melting. The experiment results have suggested that doping a small amount of Ce has little effect on oxidation kinetics of the alloy at 500 ℃ and 700 ℃ (Fig. 6 (a)), while the presence of Ce presents a palpable effect on the alloy oxidation behavior at 900-1300 ℃. Figs. 6 (b-d) provide the mass variation curves of MSB_1 and MSBCe oxidized at 900-1300 ℃, respectively. It can be seen that the mass loss of MSB_1 increases after the addition of Ce (Figs. 6 (c, d)). Even so, MSBCe exhibits shorter transient oxidation periods as compared to MSB_1, and its steady-state stage curve almost presents a horizontal trend, revealing that MSBCe is more effectively protected than MSB_1.

At the same time, the microstructural morphology of two oxidized alloys is shown in Fig. 7. During oxidation at 900 ℃, one-layered oxide film (i.e. Mo-oxide film) and flowing glassy phase are observed on the surface of both alloys (Figs. 7 (a, d)). The difference is that the glassy phase in MSBCe flows faster due to the presence of Ce, hence MSBCe presents a smaller mass variation at 900 ℃ (Fig. 6 (b)). However, after oxidation at 1100 ℃ for 24 h, the oxide-layer structure of both alloys has changed distinctly, namely SiO_2 layer is formed on top of the Mo-oxide layer (Figs. 7 (b, e)). When the oxidation temperature reaches 1300 ℃, B_2O_3 has begun to evaporate from the oxide scale, resulting in increased viscosity and weak fluidity of the scale, which leads

Preprints (www.preprints.org) | NOT PEER-REVIEWED | Posted: 31 August 2021 doi:10.20944/preprints202108.0578.v1

to the deterioration of alloy antioxidation ability [104-108]. Nevertheless, the addition of Ce increases the volatilization temperature of B_2O_3, leaving the fluidity of oxide scale largely unchanged. So the flow traces of glassy scale can still be observed on the MSBCe surface even at 1300 ℃; in contrast, the MSB_1 surface has little flow traces (Figs. 7 (c, f)). There is no doubt that scale flow can heal pores and cracks on the alloy surface, thus Ce addition has a positive effect on the oxidation protection of MSB_1.

In addition, Das et al. [109] also researched the oxidation reaction of Mo-Si-B-Al-Ce alloys at 1100 ℃. It is well known that adding Al to Mo-Si-B systems may lead to the failure of alloy oxidation protection owing to the formation of mullite [110-114], which is also verified by the mass loss curves of Al-doped alloy in Figs. 6 (b-d). Das [109] noted that adding Ce can further inhibit the malignant oxidation of Mo-Si-B-Al systems at 1100 ℃, since the presence of Ce hindered the generation of mullite and promoted the formation of dense protective Al-oxide films on the alloy surface, thereby improving the antioxidant capacity.

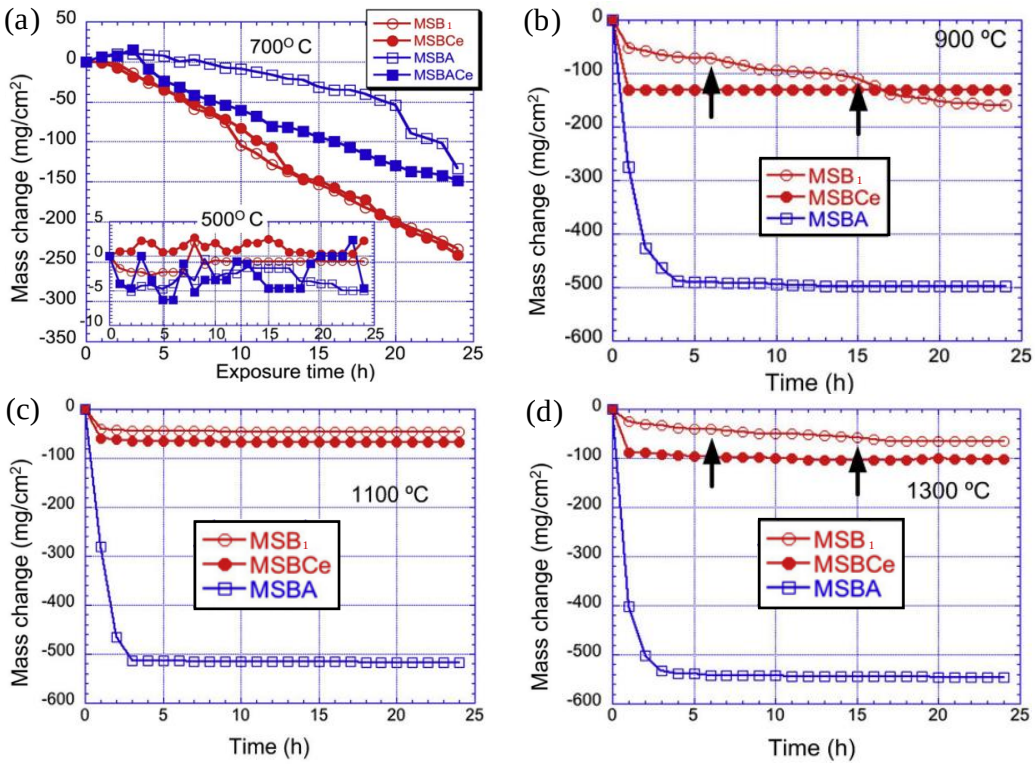

Fig. 6. Mass loss curves of various alloys at different temperatures. (a) and (b-d) reproduced with permissions [102] and [103], respectively. Copyright 2010 Elsevier and 2016 Elsevier.

Preprints (www.preprints.org) | NOT PEER-REVIEWED | Posted: 31 August 2021 doi:10.20944/preprints202108.0578.v1

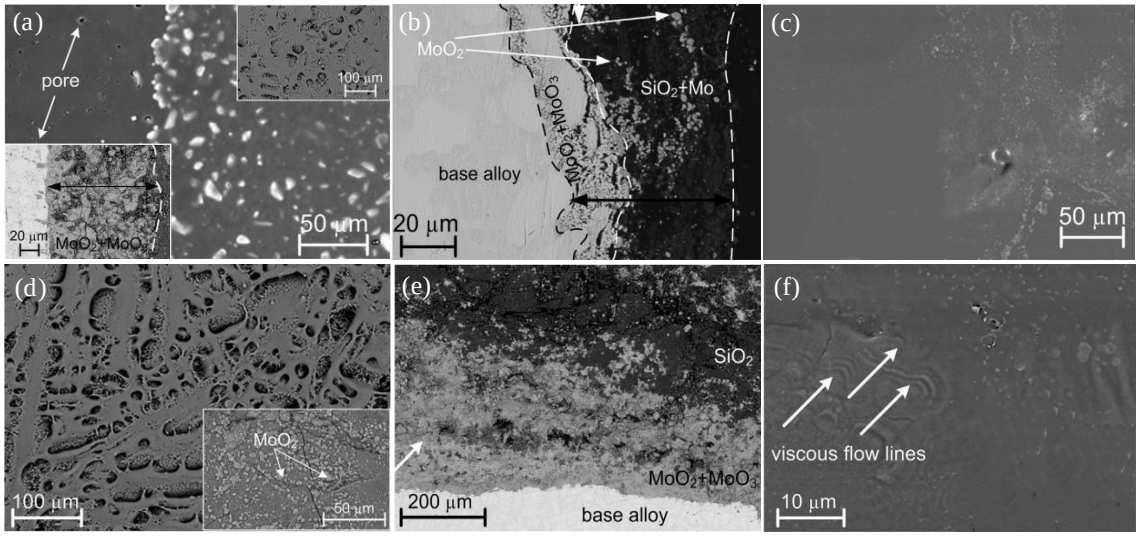

Fig. 7. Surface and cross-sectional SEM (BSE) images of MSB_1 (a-c) and MSBCe (d-f) alloys oxidized at different temperatures for 24 h: 900 ℃ (a, d), 1100 ℃ (b, e) and 1300 ℃ (c, f). Reproduced with permission [103]. Copyright 2016 Elsevier.

2.1.4 Effects of Y element addition

It has been sure that adding Y element can significantly prolong the service life of Mo-based alloys due to the fact that Y will exhibit higher oxygen affinity than Mo [115, 116]. Moreover, Y can also inhibit ion diffusion in grain boundaries and decrease the oxide-scale growth rate [117-119]. The presence of Y improves the adhesion between oxide film and substrate, thus improving the alloyed oxidation resistance [120, 121]. Therefore, researchers try to add Y element to Mo-Si-B alloys to obtain materials with better performance. After comparing the variation of Y-doped and Y-free Mo-9Si-8B (at.%) samples in the oxidation behavior at 650-1400 ℃, Majumdar et al. [122-124] found that all samples presented a trend of transient mass increase followed by continuous rapid decrease at 650 ℃ (Fig. 8 (a)). Among all the samples, the 2at.% Y-doped sample had the minimum mass loss at 750-1000 ℃ (Figs. 8 (b-e)), and the 0.2at.% Y-doped sample presented the lowest mass loss at 1100 ℃ (Fig. 8 (f)). This is because the addition of Y can produce stable Y_6MoO_{12} and $Y_5Mo_2O_{12}$ oxides at the initial period of oxidation, which can inhibit the generation and vaporization of MoO_3, leading to a decrease in the mass loss of the samples containing Y.

Preprints (www.preprints.org) | NOT PEER-REVIEWED | Posted: 31 August 2021 doi:10.20944/preprints202108.0578.v1

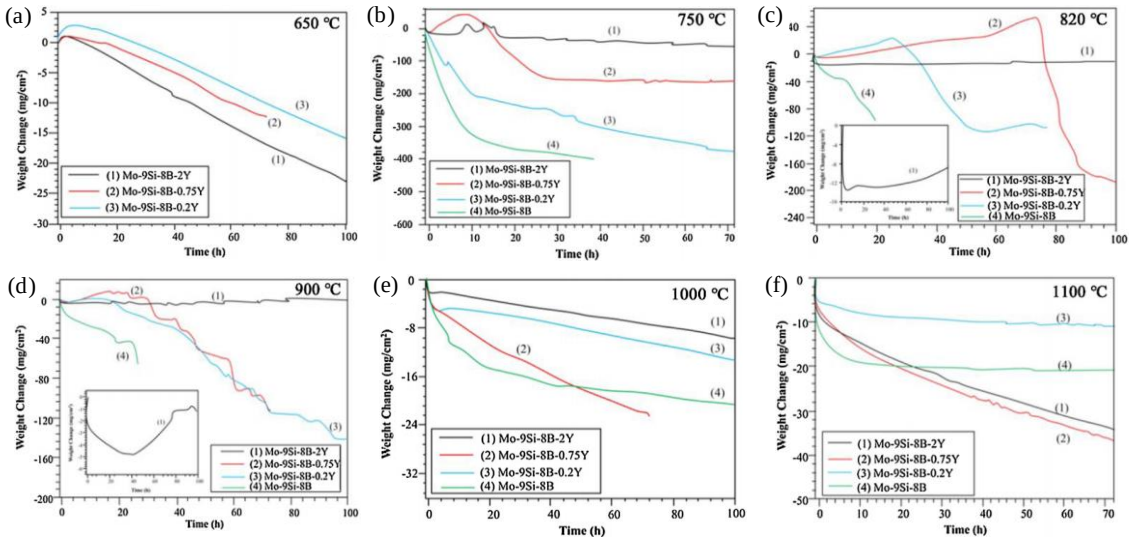

Fig. 8. Weight change curves of Y-doped and undoped samples oxidized at 650 ℃-1100 ℃, respectively. Reproduced with permission [122]. Copyright 2014 Elsevier.

In order to further clarify the role of Y doping on the sample antioxidation behavior, the microstructure of oxidized samples are analyzed in detail [58, 122]. Figs. 9 (a, b) give the cross-sectional micrographs of 2at.% and 0.75at.% Y-doped samples oxidized at 900 ℃ for 24 h, respectively. It can be seen that 0.75at.% Y-doped sample has a thicker inner MoO_2 scale than that of 2at.% Y-doped sample, which indicates that properly increasing the concentration of Y can inhibit the formation of MoO_2 to some extent. Furthermore, microcracks are also observed on the outer SiO_2 scale of 0.75at.% Y-doped sample due to the quite high growth velocity (about 7.6 $\mu m \cdot h^{-1}$) of inner MoO_2 scale, which produces such a large tensile stress that outer SiO_2 scale breaks (Figs. 9 (b, d)). It is worth noting that the thickness of inner MoO_2 scale for 0.75at.% Y-doped sample is significantly thinner after oxidation at 1100 ℃ for 72 h (Fig. 9 (c)). Because SiO_2 will present viscous flow to cover holes and cracks on the alloy surface during the temperature exceeds 965 ℃ [125, 126], which prevents further oxidation of the substrate. Fig. 9 (e) shows the thickness changes of SiO_2 and MoO_2 layers for 0.2at.% Y-dpoed sample at 1100 ℃ and 1200 ℃, which further supports the above analysis results. When the oxidation temperature is higher than 1200 ℃, a thin yttrium-silicate ($Y_2Si_2O_7$) scale is observed on the outer surface of Y-doped samples (Figs. 10 (a-d)), and the thickness of yttrium-silicate film gradually increases as the oxidation temperature raises (Figs. 10 (c, e)) [123]. It has been proved that the outer yttrium-silicate film is conducive to the alloy oxidation protection through preventing SiO_2 from forming volatile silicon hydroxide in humid conditions above 1200 ℃ [127-129]. Similar studies have been reported by Gorr et al. [130]

Preprints (www.preprints.org) | NOT PEER-REVIEWED | Posted: 31 August 2021 doi:10.20944/preprints202108.0578.v1

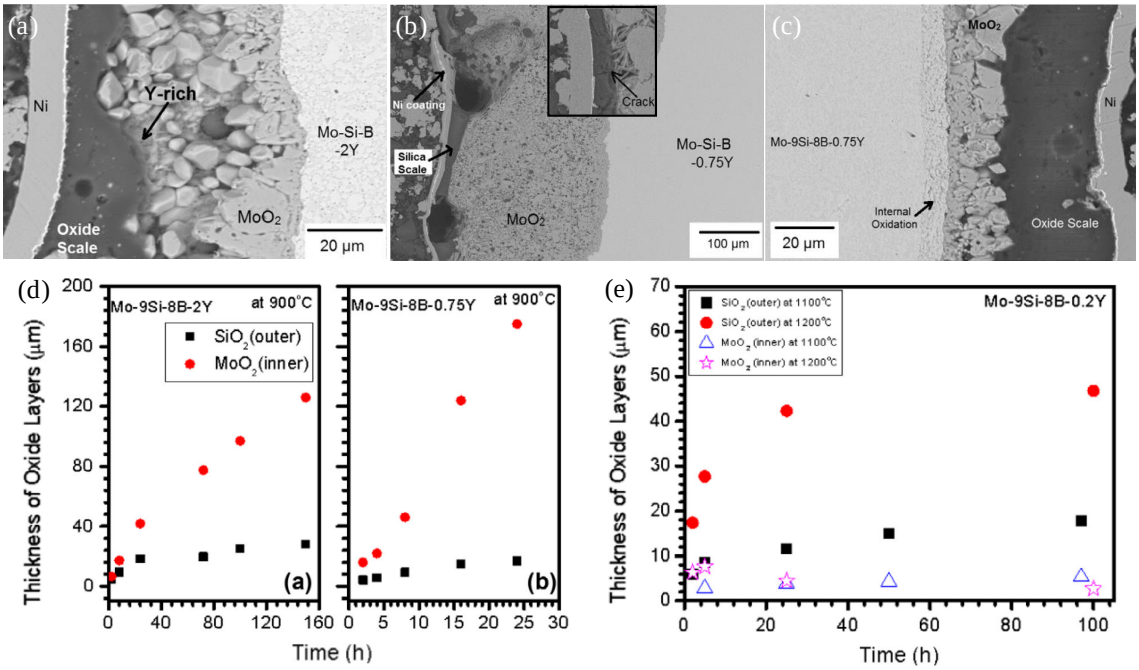

Fig. 9. Cross-sectional BSE images of 2at.% and 0.75at.% Y-doped samples oxidized at differernt conditions: (a, b) 900 ℃ for 24 h, (c) 1100 ℃ for 72 h; (d, e) Changes of MoO_2 laye and SiO_2 layer thickness in Y-doped samples oxidized at different temperatures. Reproduced with permission [122]. Copyright 2014 Elsevier.

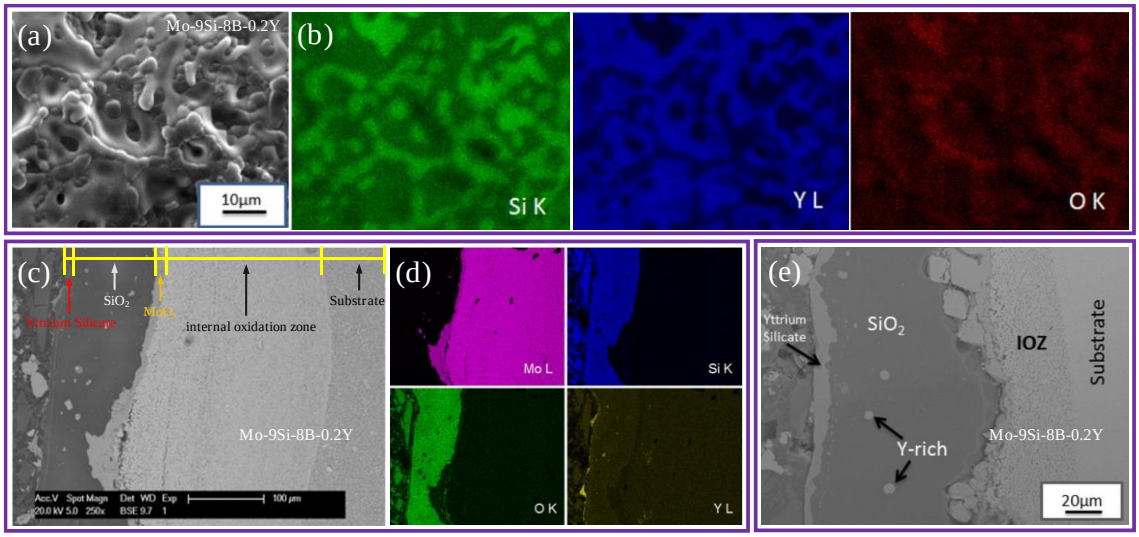

Fig. 10. Surface SE (a) and cross-sectional BSE (c, e) images of 0.2at.% Y-doped samples oxidized at differernt conditions: 1300 ℃ for 100 h (a, c) and 1400 ℃ for 2 h (e); (b, d) are the element mappings of (a, c), respectively. Reproduced with permission [123]. Copyright 2013 Springer Nature.

There is no doubt that alloying with Zr has a great impact on the antioxidant ability of Mo-Si-B materials. This is because the addition of Zr may produce polymorphic ZrO_2 or monomorphic $ZrSiO_4$, which mainly depends on the oxidation temperature. Among them, the $ZrSiO_4$ can act as an obstacle phase, which is

Preprints (www.preprints.org) | NOT PEER-REVIEWED | Posted: 31 August 2021 doi:10.20944/preprints202108.0578.v1

beneficial to improve the alloy oxidation behavior; whereas the ZrO_2 will expand in volume at high temperatures (>1200 ℃), which destroys the integrity of SiO_2 scale so that it loses the protective effect [131, 132]. Therefore, inhibiting the formation of ZrO_2 phase is essential to improve the alloy oxidation resistance.

Based on the fact that yttria suppresses the zirconia phase transition [133, 134], Yang et al. [135] designed and fabricated Mo-12Si-10B-1Zr-0.3Y, Mo-12Si-10B-1Zr and Mo-12Si-10B samples (at.%, abbreviated as 1Zr-0.3Y, 1Zr-0Y and 0Zr-0Y, respectively). Fig. 11 (a) shows the mass variation of the three samples at 1250 ℃, it can be seen that adding 1at.% Zr to the 0Zr-0Y sample will lead to continuous and sharp mass loss. Because the 0Zr-0Y sample has formed dense protective SiO_2 films during the oxidation, which avoids the sample sustained mass loss (Fig. 12 (a)), whereas the addition of Zr causes the SiO_2 scale to become loose and porous due to the formation of ZrO_2, and the porous structure provides channels for O_2 inward diffusion, thus accelerating the sample oxidation (Fig. 12 (b)). It is encouraging that further adding 0.3at.% Y can effectively prevent the rapid mass loss of 1Zr-0Y sample. As can be seen from Fig. 12 (c), $ZrSiO_4$ rather than ZrO_2 appears on the sample surface after the addition of Y, thus eliminating the adverse effect of Zr doping. Meantime, the Y-Mo-rich oxide is also observed around $ZrSiO_4$ phase. EDS analysis shows that the Y/Mo atomic ratio of this oxide is about 1/2, revealing that the oxide may be $Y_2Mo_4O_{15}$. Again, the XPS spectra also presents that the oxide has nearly the same Mo 3d and Y 3d bonding energies as $Y_2Mo_4O_{15}$ gauged through You et al. [136], which further verifies the above inference (Figs. 11 (b, c)). What's more, the 1Zr-0.3Y sample surface also forms a uniformly dense outer $Y_2Si_2O_7$ scale with the increase of oxidation time, which provides a better protection effect than 0Zr-0Y sample (Fig. 12 (d)). It has been observed from the cross-section enlarged Figs. 12 (e, f) that Y diffuses outward with the metastable $Y_2Mo_4O_{15}$ as the carrier and produces $Y_2Si_2O_7$ after a series of reactions at the top of SiO_2 scale, which will be accumulated and compressed to form the outer $Y_2Si_2O_7$ layer. Therefore, 1Zr-0.3Y sample presents the best antioxidant performance among the three samples.

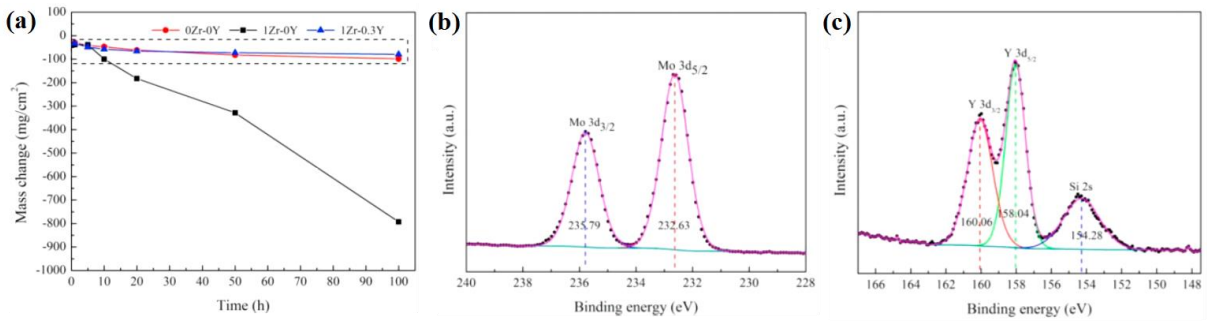

Fig. 11. Mass change curves of three studied sampes at 1250 °C (a); XPS analysis of Mo (b) and Y (c) characterized the 1Zr-0.3Y sampe surface oxidized for 1 h. Reproduced with permission [135]. Copyright 2020 Elsevier.

Preprints (www.preprints.org) | NOT PEER-REVIEWED | Posted: 31 August 2021 doi:10.20944/preprints202108.0578.v1

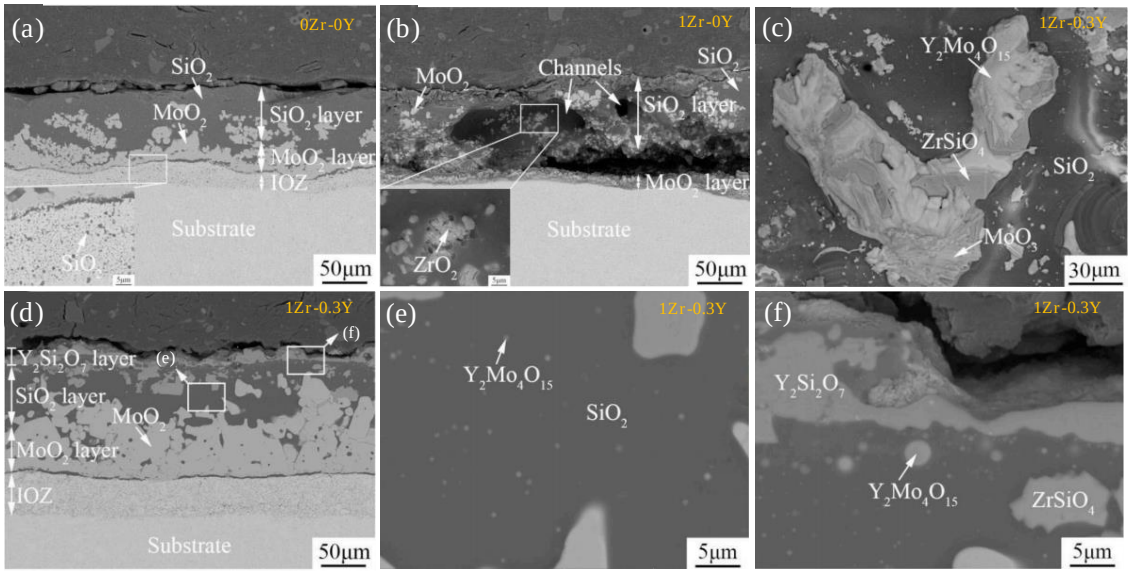

Fig. 12. Cross-sectional and surface BSE images of three studied sampes oxidized at 1250 ℃ for different time: (a) 20 h, (b) 5 h, (c) 1 h, (d-f) 50 h. Reproduced with permission [135]. Copyright 2020 Elsevier.

2.2 Effects of rare earth elements on oxidation behavior of other Mo-Si alloys

Previous studies have pointed out that adding Nb to the Mo-Si-based materials can play a satisfactory effect in improving mechanical properties due to damaging the stability of Mo_3Si phase [137-139]. However, the presence of Nb will lead to catastrophic oxidation of the material [140-142]. Inspired by the above study that adding Y can enhance the antioxidant properties of Zr-doped Mo-Si-B alloys, we further discussed the role of adding Y on the oxidation behavior of Nb-doped Mo-Si alloys.

Majumdar [143] used the nonconsumable arc-melted method to prepare the undoped and 0.5Y-doped Mo-26Nb-19Si samples (at.%), which simply referred to as Alloy1 and Alloy2, respectively. The microstructures of both samples are shown in Figs. 13 (a, e). It can be found that they are both composed of dark and bright areas. According to XRD analysis (Fig. 14 (a)) and EBSD mappings (Figs.13 (b-d, f-h)), the dark and bright areas are $(Mo, Nb)_5Si_3$ and $(Mo, Nb)_{ss}$ phases, respectively. Moreover, Y_2O_3 particles are also observed on the Alloy2 grain boundaries. These particles can suppress the elongated grain growths, which results in the difference of microstructure morphology between the two samples. Meanwhile, Majumdar [143] also studied the oxidation process of Alloy2 at 1000 ℃ and 1300 ℃. It is established that the sample exhibits continuous linear mass loss when oxidized at 1000 ℃. When the oxidation temperature increases to 1300 ℃, the sample is oxidized more vigorously and loses its antioxidant capacity within 2 h of oxidation, as shown in Fig. 14 (b). Fig. 15 shows the cross-section and surface micrographs of the oxidized sample. It can be discovered that the Alloy2 surface has formed a thick oxide layer after oxidation at 1000 ℃ for 24h (Fig. 15 (a)). As can be seen

Preprints (www.preprints.org) | NOT PEER-REVIEWED | Posted: 31 August 2021 doi:10.20944/preprints202108.0578.v1

from Fig. 15 (d), the oxide layer is mainly composed of MoO_2, Nb_2O_5 and SiO_2, wherein Nb_2O_5 can act as a channel for O_2 internal diffusion due to the lack of protective action, which leads to rapid oxidation of the sample. In addition, the sample surface oxide film, which consists of Y_2O_3, Nb_2O_5 and SiO_2, appears numerous cracks and holes during oxidation at 1300 ℃ for 2 h (Figs. 15 (b, c)), resulting in the loss of protection from oxidation. Therefore, adding Y to Mo-Si-Nb alloys cannot overcome the oxidizing problem.

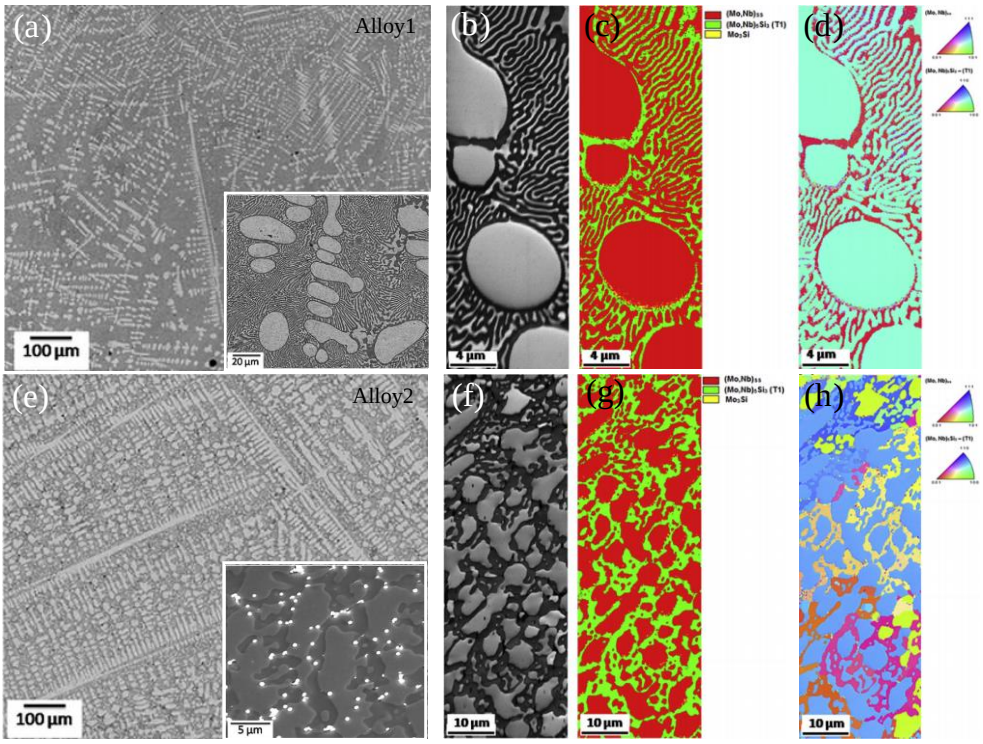

Fig. 13. Microstructure morphologies of Alloy1 (a) and Alloy2 (e); EBSD mappings of Alloy1 and Alloy2: band contrast (b, f), phase (c, g), IPF (d, h). Reproduced with permission [143]. Copyright 2018 Elsevier.

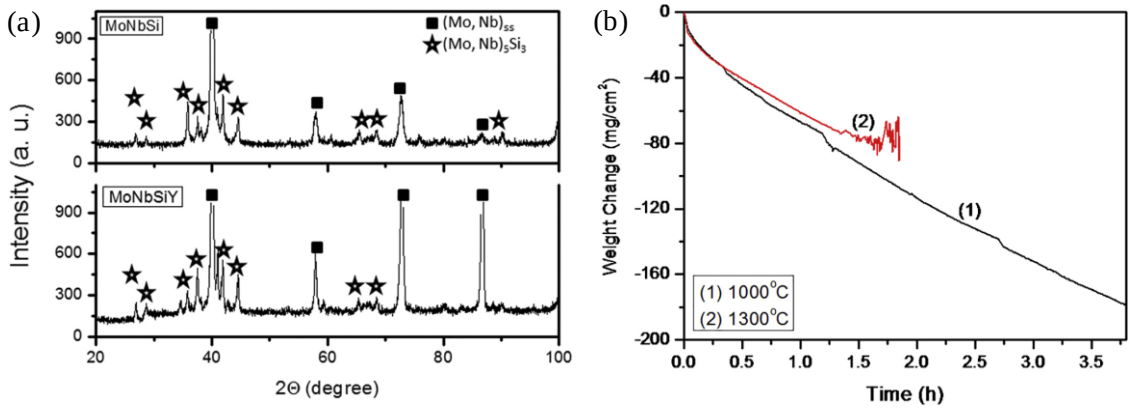

Fig. 14. (a) XRD patterns of both samples before the oxidation; (b) Weight change curves of Alloy2 oxidized at 1000 ℃ and 1300 ℃, respectively. Reproduced with permission [143]. Copyright 2018 Elsevier.

Preprints (www.preprints.org) | NOT PEER-REVIEWED | Posted: 31 August 2021 doi:10.20944/preprints202108.0578.v1

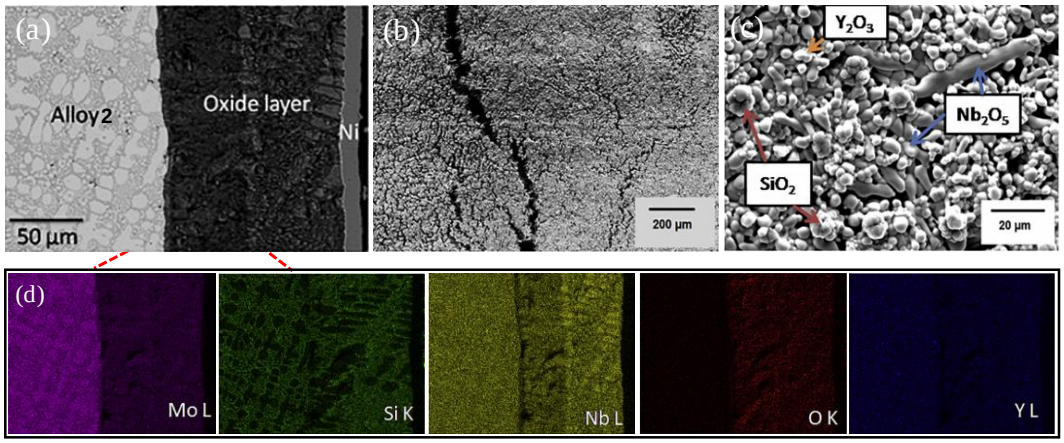

Fig. 15. Cross-section BSE micrograph of Alloy2 (a) with the corresponding EDS mappings (d) oxidized at 1000 ℃ for 24 h; Surface SEM/SE images of low (b) and high magnifications (c) for Alloy2 oxidized at 1300 ℃ for 2 h. Reproduced with permission [143]. Copyright 2018 Elsevier.

3. Strengthening mechanism of rare earth elements

According to the above research, it can be determined that the improvement of oxidation behavior of Mo-Si-based alloys by rare earth elements is mainly achieved through the following three ways. First, optimizing the microstructure of the alloy is caused by refining grains or distributing phase compositions uniformly, which contributes to the rapid formation of oxide scale [80, 96, 103, 144]. Second, producing stable rare earth oxides, these oxides are dispersed in scale and act as obstacle phases or diffusion barriers, which is conducive to suppressing the MoO_3 volatilization and O_2 inward diffusion [59, 122, 123]. Third, forming an additional rare earth oxide layer, thus further improving the antioxidant capacity [96, 135].

Fig. 16 shows a schematic diagram of the oxidation process for rare earth element doped and undoped Mo-Si-based alloys at medium-high temperatures, which is helpful to further understand the strengthening mechanism of rare earth elements. It can be seen that the alloy with finer grain size can be prepared after adding rare earth elements like La, which will affect the oxidation behavior to some extent. Overall, the oxidation process of the two kinds of alloys can be divided into two stages: initial and stable oxidation stages. During the initial oxidation stage, a discontinuous SiO_2 scale is formed on the surface of alloy without rare earth doping, which cannot effectively isolate oxygen. As a result, the alloy is oxidized violently and forms a Mo-oxide (MoO_2 and MoO_3) layer below the SiO_2 scale. Among them, MoO_3 is highly volatile, which leads to a severe mass loss of the alloy and leaves some holes and cavities on the surface [145]. Fortunately, SiO_2 gradually increases and flows to heal these holes and cavities as the oxidation time increases, thus facilitating the formation of continuous SiO_2 scale [146]. During the stable oxidation stage, the complete scale can provide

Preprints (www.preprints.org) | NOT PEER-REVIEWED | Posted: 31 August 2021 doi:10.20944/preprints202108.0578.v1

sufficient protection for the substrate due to the effective restriction of O_2 internal diffusion, resulting in the reduction of oxygen pressure inside the alloy. Obviously, low oxygen partial pressure inhibits the continuous generation of MoO_2, and the original MoO_2 will continue to oxidize to produce MoO_3 and slowly volatilize so that the Mo-oxide interlayer becomes thinner [147]. Meanwhile, the substrate below MoO_2 layer has been oxidized selectively, leading to the emergence of internal oxidation zone [122], as shown in Fig. 16 (a). In contrast, the alloy doped with rare earth can generate rare earth oxides such as La_2O_3, Y_6MoO_{12}, $Y_5Mo_2O_{12}$, etc. in the initial oxidation stage. These stable oxides, on the one hand, promote the formation of continuous SiO_2 scale. On the other hand, they fill holes in the scale to eliminate the shortcut of O_2 inward diffusion and MoO_3 volatilization, so that the alloy can enter the stable oxidation stage faster. In addition, a double-layer protective oxide film (i.e. $Y_2Si_2O_7$-SiO_2 or SiO_2-$HfSiO_4$ duplex scales) is formed on the alloy surface during the stable oxidation stage, providing more effective protection against oxidation, as shown in Fig. 16 (b).

However, it is disappointing that sometimes the addition of rare earth elements may even lead to the deterioration of alloy oxidation behavior in high temperature environments. For example, adding La to the Mo-Si-B system above 1100 ℃ has leaded to its accelerated oxidation attribute to the formation of large amounts of cracks and holes [60]. Therefore, the challenges ahead remain severe.

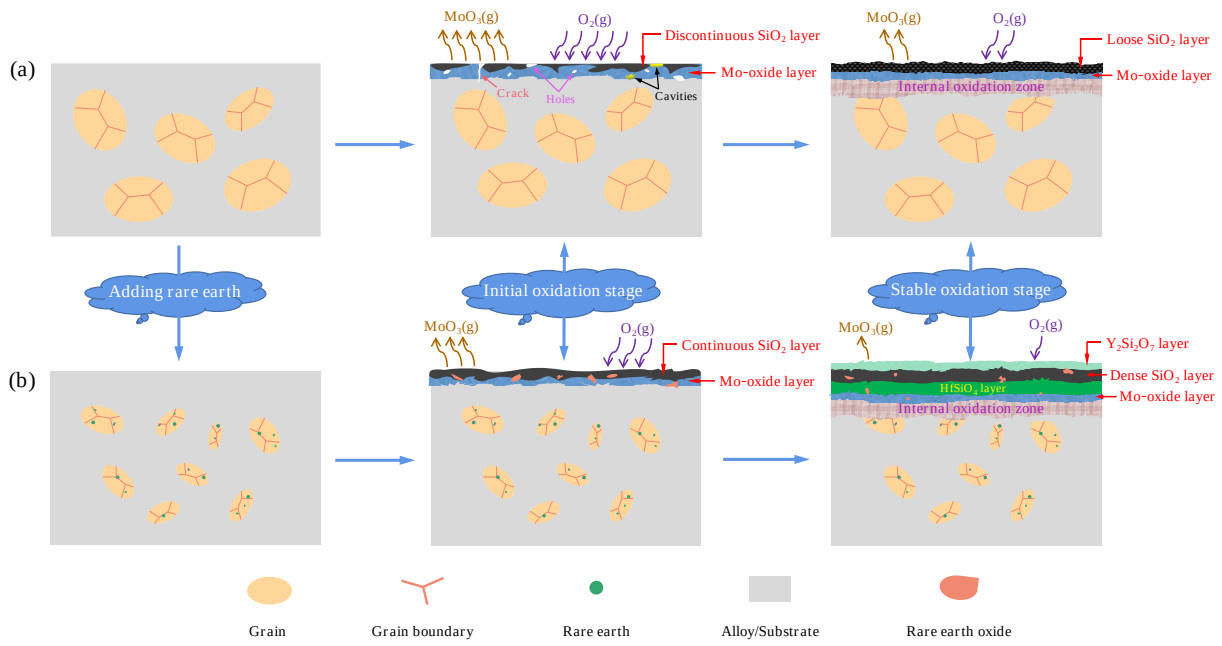

Fig. 16. Schematic diagram of the oxidation process for Mo-Si-based alloy at medium-high temperature: (a) without rare earth elements, (b) doped with rare earth elements.

Preprints (www.preprints.org) | NOT PEER-REVIEWED | Posted: 31 August 2021 doi:10.20944/preprints202108.0578.v1

4. Conclusion and outlook

This paper comprehensively reviewed the role of rare earth elements on the oxidation behavior of Mo-Si-based alloy. Based on the thorough study about the oxidation process of Mo-Si-based alloy, the strengthening mechanism of various rare earth elements such as La, Hf, Ce and Y was summarized. The addition of La to Mo-Si-B alloys can make grains become finer to promote the rapid formation of continuous boroilicate scales; Meantime, producing stable La-containing oxides with a "pinning" effect like $3La_2O_3 \cdot MoO_3$, La_2O_3 and $La_2O_3 \cdot 3MoO_3$, which limits the formation and evaporation of MoO_3, thus significantly enhancing the alloy oxidation resistance at temperatures below 1000 ℃. Mo-Si-B alloys doped with Hf can generate $HfSiO_4$ particles that promote the healing of holes and cracks in oxide scales; Besides, it is likely that $HfSiO_4$ inner layer will be formed to inhibit the MoO_3 volatilization and O_2 inward diffusion. These are helpful to improve the antioxidant capacity of the alloy. Alloying with Ce can shorten the transient oxidation period of Mo-Si-B alloys; Moreover, the presence of Ce can also raise the volatilization temperature of B_2O_3 in oxide films, which plays a positive role in maintaining the viscosity and integrity of borosilicate scale. It is worth mentioning that the addition of Ce to the Mo-Si-B-Al system can also hinder the formation of mullite and promote the emergence of protective Al-oxide scale, thus providing more effective protection against oxidation. Adding Y can passivate Mo-Si-B alloys to prevent further oxidation. On the one hand, the existence of Y will produce stable Y-Mo-rich oxides (Y_6MoO_{12}, $Y_5Mo_2O_{12}$, etc.), which suppresses the formation of MoO_3 and accelerates the nucleation and growth of protective SiO_2 scales; On the other hand, a $Y_2Si_2O_7$ outer layer is created which acts as a diffusion barrier. Furthermore, adding Y to the Mo-Si-B-Zr system also suppresses ZrO_2 formation, thus eliminating the adverse effect of Zr doping on oxidation behavior.

However, it is noteworthy that adding rare earth elements do not always improve the antioxidation ability of Mo-Si-based alloys in practice. For example, adding Y to the Mo-Si-Nb system cannot prevent its catastrophic oxidation; The addition of La also causes deterioration in the oxidation behavior of Mo-Si-B alloys above 1000 ℃. Therefore, a further search for other oxidation protection methods is necessary. Some research schemes worth exploring in the future are listed below, hoping to help solve the problems encountered in the practical application of Mo-Si-based alloys. Before using, preoxidation treatment at an appropriate temperature can obtain protective silica scales on the alloy surface, thus effectively inhibiting the inward diffusion of O_2 and obviously extending the service life of alloy. Processing of preceramic polymers is a very promising method owing to its simple operation and low cost. Preceramic polymers, which mainly includes many silicon-containing ceramic precursors like polysilazanes, polycarbosilanes and polysiloxanes, can be decomposed into

 doi:10.20944/preprints202108.0578.v1

SiC, SiCN, SiCO or Si_3N_4 to form protective silica scales at high temperature environments, thereby exhibiting the excellent antioxidant properties. Considering the type, concentration, chemical activity, selective oxidation and other factors of elements in the alloy, relevant numerical simulation or mathematical model is established to quantitatively study the relationship between oxidation behavior and microstructure. Combined with the emerging coating technology to design a suitable silicide-based coating such as $MoSi_2$ ceramic coating for the Mo-Si-based system, which will help to provide a superior antioxidant capability.

Corresponding Authors

Corresponding author: Yingyi Zhang (Y.Y. Zhang)

E-mail : zhangyingyi@cqu.edu.cn (Y.Y. Zhang), Tel.: +86 17375076451

Author Contributions:

The manuscript was written through the contributions of all authors. Y.Y. Zhang: Conceptualization, Investigation, and Supervision. Y.Y. Zhang and L.H. Yu: Writing original draft and image processing. L.H. Yu, T. Fu, K.K. Cui, and F.Q. Shen: Validation, Resources, Investigation, Writing- review & editing. Y.Y. Zhang, L.H. Yu and J. wang: Visualization, Writing - review & editing. All authors have given approval to the final version of the manuscript.

Notes

The authors declare no competing financial interest.

Acknowledgments

This work was supported by the National Natural Science Foundation of China (No.51604049).

References

[1] J. Wang, Y.Y. Zhang, K.K. Cui, T. Fu, J.J. Gao, S. Hussain, T.S. AlGarni. Pyrometallurgical recovery of zinc and valuable metals from electric arc furnace dust – A review, Journal of Cleaner Production. 298 (2021): 126788.

[2] M.A. Azim, S. Burk, B. Gorr, H.J. Christ, D. Schliephake, M. Heilmaier, R. Bornemann, P.H. Bolívar. Effect of Ti (Macro-) alloying on the high-temperature oxidation behavior of ternary Mo-Si-B alloys at 820–1300°C, Oxidation of Metals. 80 (2013): 231-242.

[3] D. Schliephake, C. Gombola, A. Kauffmann, M. Heilmaier, J.H. Perepezko. Enhanced oxidation resistance of Mo-Si-B-Ti alloys by pack cementation, Oxidation of Metals. 88(3-4) (2017): 267-277.

[4] D. Schliephake, M. Azim, K.V. Klinski-Wetzel, B. Gorr, H.J. Christ, H. Bei, E.P. George, M. Heilmaier. High-

temperature creep and oxidation behavior of Mo-Si-B alloys with high Ti contents, Metallurgical and Materials Transactions A. 45(3) (2014): 1102-1111.

[5] J.A. Lemberg, R.O. Ritchie. Mo-Si-B alloys for ultrahigh-temperature structural applications, Advanced Materials. 24(26) (2012): 3445-3480.

[6] J.H. Perepezko. The hotter the engine, the better, Science. 326(5956) (2009): 1068-1069.

[7] J.C. Zhao. J.H. Westbrook. Ultrahigh-temperature materials for jet engines, Mrs Bulletin. 28(09) (2003): 622-630.

[8] A.M. Meyer, M.J. Kramer, A.J. Thom, J.J. Huebsch, B. Cook. Structural materials: properties, microstructure and processing, Materials Science and Engineering: A. 261 (1999): 16-8.

[9] J.J. Huebsch, M.J. Kramer, H.L. Zhao, M. Akinc. Solubility of boron in $Mo_{5+y}Si_{3-y}$, Intermetallics. 8 (2000): 143-50.

[10] J. Becker, D. Fichtner, S. Schmigalla, S. Schultze, C. Heinze, Y. Küsters, G. Hasemann, J. Schmelzer, M. Krüger. Oxidation response of additively manufactured eutectic Mo-Si-B alloys, IOP Conf. Series: Materials Science and Engineering. 882 (2020): 012002.

[11] L. Ingemarsson, K. Hellström, S. Čanović, T. Jonsson, M. Halvarsson, L.G. Johansson, J.E. Svensson. Oxidation behavior of a $Mo(Si,Al)_2$ composite at 900-1600°C in dry air, Journal of Materials Science. 48(4) (2013): 1511-1523.

[12] J.J. Petrovic. Mechanical behavior of $MoSi_2$ and $MoSi_2$ composites, Materials Science and Engineering: A. 192-193(1) (1995): 31-37.

[13] J.H. Schneibel, J.A. Sekhar. Microstructure and properties of $MoSi_2$-MoB and $MoSi_2$-Mo_5Si_3 molybdenum silicides, Materials Science and Engineering: A. 340(1-2) (2003): 204-211.

[14] M. Zhao, B.Y. Xu, Y.M. Shao, J.F. Liang, S.S. Wu, Y.W.Yan. Oxidation behavior of Mo_{ss}-Ti_5Si_3-T_2 composites at intermediate and high temperatures, Intermetallics. 118 (2020): 106702.

[15] A.K. Vasudévan, J.J. Petrovic. A comparative overview of molybdenum disilicide composites, Materials Science and Engineering A. 155(1-2) (1992): 1-17.

[16] H. Zhang, D.Z. Wang, S.P. Chen, X.Y. Liu. Toughening of $MoSi_2$ doped by La_2O_3 particles, Materials Science and Engineering: A. 345(1-2) (2003): 118-121.

[17] S.H. Wen, C.G. Zhou, J.B. Sha. Improvement of oxidation resistance of a Mo-62Si-5B (at.%) alloy at 1250°C and 1350°C via an in situ pre-formed SiO_2 fabricated by spark plasma sintering, Corrosion Science. 127 (2017): 175-185.

[18] Y.Y. Zhang, J. Zhao, J.H. Li, J. Lei, X.K. Cheng. Effect of hot-dip siliconizing time on phase composition and

microstructure of Mo-$MoSi_2$ high temperature structural materials, Ceramics International. 45(5) (2019): 5588-5593.

[19] K. Ito, T. Hayashi, M. Yokobayashi, H. Numakura. Evolution kinetics and microstructure of $MoSi_2$ and Mo_5Si_3 surface layers on two-phase Mo-9Si-18B alloy during pack-cementation and high-temperature oxidation, Intermetallics. 12(4) (2004): 407-415.

[20] B.A. Pint, On the formation of interfacial and internal voids in a-Al_2O_3 scales, Oxidation of Metals. 48 (1997): 303-328.

[21] S. Lohfeld. Oxidation behaviour of particle reinforced $MoSi_2$ composites at temperatures up to 1700°C. Part II: Initial screening of the oxidation behaviour of $MoSi_2$ composites, Materials and Corrosion. 56(3) (2005): 149-158.

[22] S. Lohfeld, M. Schütze, A. Böhm, V. Güther. Oxidation behaviour of particle reinforced $MoSi_2$ composites at temperatures up to 1700°C. Part III: Oxidation behaviour of optimised $MoSi_2$ composites, Materials and Corrosion. 56(4) (2005): 250-258.

[23] J.J. Petrovic, A.K. Vasudevan. Key developments in high temperature structural silicides, Materials Science and Engineering: A. 261(1-2) (1999): 1-5.

[24] Y.Y. Zhang, Y.G. Li, C.G. Bai. Microstructure and oxidation behavior of Si-$MoSi_2$ functionally graded coating on Mo substrate, Ceramics International. 43(8) (2017): 6250-6256.

[25] Y.Y. Zhang, J.M. Qie, K.K. Cui, T. Fu, X.L. Fan, J. Wang, X. Zhang. Effect of hot dip silicon-plating temperature on microstructure characteristics of silicide coating on tungsten substrate, Ceramics International. 46(4) (2020): 5223-5228.

[26] J.J Petrovic. Toughening strategies for $MoSi_2$-based high temperature structural silicides, Intermetallics. 8(9-11) (2000): 1175-1182.

[27] T. Sossaman, R. Sakidja, J.H. Perepezko. Influence of minor Fe addition on the oxidation performance of Mo-Si-B alloys, Scripta Materialia. 67(11) (2012): 891-894.

[28] S. Burk, B. Gorr, M. Krüger, M. Heilmaier. Oxidation behavior of Mo-Si-B-(X) alloys: Macro- and microalloying (X=Cr, Zr, La_2O_3), JOM: the journal of the Minerals, Metals and Materials Society. 63(12) (2011): 32-36.

[29] P. Mandal, A.J. Thom, M.J. Kramer, V. Behrani, M. Akinc. Oxidation behavior of Mo-Si-B alloys in wet air, Materials Science and Engineering A. 371 (2004): 335-342.

[30] Y.L. Jeng, E. Lavernia. Processing of molybdenum disilicide, Journal of Materials Science. 29(10) (1994): 2557-2571.

[31] D.G. Morris, M. Leboeuf, M.A. Morris. Hardness and toughness of $MoSi_2$ and $MoSi_2$-SiC composite prepared

by reactive sintering of powders, Materials Science and Engineering: A. 251(1-2) (1998):262-268.

[32] A. Chrysanthou, R.C. Jenkins, M.J. Whiting, P. Tsakiropoulos. A study of the combustion synthesis of $MoSi_2$ and $MoSi_2$-matrix composites, Journal of Materials Science. 31(16) (1996): 4221-4226.

[33] S. Ignat, P. Sallamand, A. Nichici, A.B. Vannes, D. Grevey, E. Cicală. $MoSi_2$ laser cladding-a comparison between two experimental procedures: Mo-Si online combination and direct use of $MoSi_2$, Optics and Laser Technology. 33(7) (2001): 461-469.

[34] T. Fu, K.K. Cui, Y.Y. Zhang, J. Wang, X. Zhang, F.Q. Shen, L.H. Yu, H.B. Mao. Microstructure and oxidation behavior of antioxidation coatings on Mo-based alloys through HAPC process: A review, Coatings. 11(8) (2021): 883.

[35] F. Wang, A.D. Shan, X.P. Dong, J.S. Wu. Microstructure and oxidation resistance of laser-remelted Mo-Si-B alloy, Scripta Materialia. 56(9) (2007): 737-740.

[36] A. Petitbon, L. Boquet, D. Delsart. Laser surface sealing and strengthening of zirconia coatings, Surface and Coatings Technology. 49(1-3) (1991): 57-61.

[37] Y.Y. Zhang, K.K. Cui, T. Fu, J. Wang, J.M. Qie, X. Zhang. Synthesis WSi_2 coating on W substrate by HDS method with various deposition times, Applied Surface Science. 511(6) (2020): 145551.

[38] Y.Y. Zhang, T. Fu, K.K. Cui, F.Q. Shen, J. Wang, L.H. Yu, H.B. Mao. Evolution of surface morphology, roughness and texture of tungsten disilicide coatings on tungsten substrate, Vacuum. 191(12) (2021): 110297.

[39] K.K. Cui, T. Fu, Y.Y. Zhang, J. Wang, H.B. Mao, T.B. Tan. Microstructure and mechanical properties of $CaAl_{12}O_{19}$ reinforced Al_2O_3-Cr_2O_3 composites, Journal of the European Ceramic Society. 2021.

[40] S. Lohfeld, M. Schütze. Oxidation behaviour of particle reinforced $MoSi_2$ composites at temperatures up to 1700 °C Part I: Literature review, Materials and Corrosion. 56(2) (2005): 93-97.

[41] Y. Suzuki, T. Sekino, K. Niihara. Effects of ZrO_2 addition on microstructure and mechanical properties of $MoSi_2$, Scripta Metallurgica et Materialia. 33(1) (1995): 69-74.

[42] P.Y. Hou, J. Stinger, The effect of reactive element additions on the selective oxidation, growth and adhesion of chromia scales, Materials Science and Engineering: A. 202(1-2) (1995): 1-10.

[43] M. Krüger, S. Franz, H. Saage, M. Heilmaier, J.H. Schneibel, P. Jéhanno, M. Böning, H. Kestler. Mechanically alloyed Mo-Si-B alloys with a continuous α-Mo matrix and improved mechanical properties, ntermetallics. 16(7) (2008): 933-941.

[44] R.J. Christensen, V.K. Tolpygo, D.R. Clarke. The influence of the reactive element yttrium on the stress in alumina scales formed by oxidation, Acta Materialia. 45(4) (1997): 1761-1766.

[45] A.A. Sharif. Effects of Re- and Al-alloying on mechanical properties and high-temperature oxidation of $MoSi_2$,

Journal of Alloys and Compounds. 518 (2012): 22-26.

[46] Y. Yang, H. Bei, J. Tiley, E.P. George. Re effects on phase stability and mechanical properties of Mo_{SS}+Mo_3Si+Mo_5SiB_2 alloys, Journal of Alloys and Compounds. 556 (2013): 32–38.

[47] H.M. Jin, L.N. Zhang. Rare earth effects on adhesion of Cr_2O_3 oxide scale formed on surface of Co–40Cr alloy, J Rare Earths. 19 (2001): 34-49.

[48] H. Qi, D.G. Lees, Y. He. Effect of surface-applied rare earth containing thin oxide film on high-temperature oxidation of Fe25Cr, Corrosion Science and Protection Technology. 11(4) (1999): 200-201.

[49] Y.Y. Zhang, K.K. Cui, Q.J. Gao, S. Hussain, Y. Lv. Investigation of morphology and texture properties of WSi_2 coatings on W substrate based on contact-mode AFM and EBSD, Surface and Coatings Technology. 396(12) (2020): 125966.

[50] X. Zhang, T. Fu, K.K. Cui, Y.Y. Zhang, F.Q. Shen, J. Wang, L.H. Yu, H.B. Mao. The protection, challenge, and prospect of anti-oxidation coating on the surface of niobium alloy, Coatings. 11(7) (2021): 742.

[51] Y.Y. Zhang, K.K. Cui, T. Fu, J. Wang, F.Q. Shen, X. Zhang, L.H. Yu. Formation of $MoSi_2$ and Si/$MoSi_2$ coatings on TZM (Mo-0.5Ti-0.1Zr-0.02C) alloy by hot dip silicon-plating method, Ceramics International. 47(16) (2021): 23053-23065.

[52] Y.Y. Zhang, S. Hussain, K.K. Cui, T. Fu, J. Wang, M.S. Javed, Y. Lv, B. Aslam. Microstructure and mechanical properties of $MoSi_2$ coating deposited on Mo substrate by hot dipping processes, Nanoelectronics and Optoelectronics. 14(12) (2019): 1680-1685.

[53] B.A. Pint. The oxidation behavior of oxide-dispersed β-NiAl: I. short-term performance at 1200°C, Oxidation of Metals. 49(5) (1998): 531-559.

[54] N. Hiramatsu, F.H. Stott. The effect of lanthanum on the scales developed on thin foils of Fe20Cr5Al at very high temperatures, Oxidation of Metals. 51(5) (1999): 479-494.

[55] T. Fu, K.K. Cui, Y.Y. Zhang, J. Wang, F.Q. Shen, L.H. Yu, J.M. Qie, X. Zhang. Oxidation protection of tungsten alloys for nuclear fusion applications: A comprehensive review, Journal of Alloys and Compounds. 884(1-2) (2021): 161057.

[56] B.A. Pint. Experimental observations in support of the dynamic-segregation theory to explain the reactive element effect, Oxidation of Metals. 45(1) (1996): 1-37.

[57] T.J. Nijdam, W.G. Sloof. Effect of reactive element oxide inclusions on the growth kinetics of protective oxide scales, Acta Materialia. 55(17) (2007): 5980-5987.

[58] K. Pan, Y.P. Yang, S.Z. Wei, H.H. Wu, Z.L. Dong, Y. Wu, S.Z. Wang, L.Q. Zhang, J.P. Lin, X.P. Mao. Oxidation behavior of Mo-Si-B alloys at medium-to-high temperatures, Journal of Materials Science and Technology. 60

(2021): 113-127.

[59] S. Majumdar, S. Burk, D. Schliephake, M. Krüger, H.J. Christ, M. Heilmaier. A study on effect of reactive and rare earth element additions on the oxidation behavior of Mo-Si-B system, Oxidation of Metals. 80(3-4) (2013): 219-230.

[60] S. Majumdar, B. Gorr, H.J. Christ, D. Schliephake, M. Heilmaier. Oxidation mechanisms of lanthanum-alloyed Mo-Si-B, Corrosion Science. 88 (2014): 360-371.

[61] D.P. Whittle, J. Stringer. Improvement in properties: Additives in oxidation resistance, Philosophical Transactions of Royal Society London. 295 (1980): 309-329.

[62] I.J. Bennett, W.G. Sloof. Modelling the influence of reactive elements on the work of adhesion between a thermally grown oxide and a bond coat alloy, Materials and Corrosion. 57(3) (2015): 223-229.

[63] D. Naumenko, B. Gleeson, E. Wessel, L. Singheiser, W.J. Quadakkers. Correlation between the microstructure, growth mechanism, and growth kinetics of alumina scales on a FeCrAlY alloy, Metallurgical and Materials Transactions A. 38(12) (2007): 2974-2983.

[64] A.J. Thom, E. Summers, M. Akinc. Oxidation behavior of extruded $Mo_5Si_3B_x$–$MoSi_2$–MoB intermetallics from 600°–1600°C, Intermetallics. 10(6) (2002): 555-570.

[65] F. Wang, A.D. Shan, X.P. Dong, J.S. Wu. Oxidation behavior of Mo-12.5Si-25B alloy at high temperature, Journal of Alloys and Compounds. 459(1-2) (2008): 362-368.

[66] K. Yoshimi, S. Nakatani, T. Suda, S. Hanada, H. Habazaki. Oxidation behavior of Mo_5SiB_2-based alloy at elevated temperatures, Intermetallics. 10 (2002): 407-414.

[67] L. Liu, C. Shi, C. Zhang, P.M. Voyles, J.H. Fournelle, J.H. Perepezko. Microstructure, microhardness and oxidation behavior of Mo-Si-B alloys in the Mo_{ss}+Mo_2B+Mo_5SiB_2 three phase region, Intermetallics. 116 (2020): 106618.

[68] G.J. Zhang, W. He, B. Li, Y. Zha, J. Sun. Effect of Si/B ratio on the microstructure and mechanical properties of lanthanum oxide-doped Mo-Si-B alloys, Journal of Alloys and Compounds. 577 (2013): 217-221.

[69] N.K. Kumar, J. Das, R. Mitra. Efect of moist air and minor Zr addition on oxidation behavior of arc-melted multiphase Mo-Si-B alloys in the temperature range of 1000°C–1300°C, Oxidation of Metals. 93 (2020): 483-513.

[70] B. Roy, Khushboo, J. Das, R. Mitra, S.K. Roy. Effect of oxygen partial pressure on the cyclic oxidation behavior of $Mo_{76}Si_{14}B_{10}$, Metallurgical and Materials Transactions A. 44 (2013): 2910-2913.

[71] X.Q. Yang, H. Tan, N. Lin, Z.X. Li, Y.H. He. Effects of the lanthanum content on the microstructure and properties of the molybdenum alloy, Int. Journal of Refractory Metals and Hard Materials. 61 (2016): 179-184.

[72] G.J. Zhang, Q. Dang, H. Kou, R.H. Wang, G. Liu, J. Sun. Microstructure and mechanical properties of

lanthanum oxide-doped Mo-12Si-8.5B (at%) alloys, Journal of Alloys and Compounds. 577 (2013): 493-498.

[73] G.J. Zhang, Y. Zha, B. Li, W. He, J. Sun. Effects of lanthanum oxide content on mechanical properties of mechanical alloying Mo-12Si-8.5B (at.%) alloys, Int. Journal of Refractory Metals and Hard Materials. 41 (2013): 585-589.

[74] J.H. Yan, H.A. Zhang, S.W. Tang, J.G. Xu. Room temperature mechanical properties and high temperature oxidation behavior of $MoSi_2$ matrix composite reinforced by adding La_2O_3 and Mo_5Si_3, Materials Characterization. 60(5) (2009): 447-450.

[75] H. Choe, D. Chen, J.H. Schneibel, R.O. Ritchie. Ambient to high temperature fracture toughness and fatigue-crack propagation behavior in a Mo-12Si-8.5B (at.%) intermetallic, Intermetallics. 9 (2001): 319-329.

[76] J.H. Schneibel, M.J. Kramer, O. Unal, R.N. Wright. Processing and mechanical properties of a molybdenum silicide with the composition Mo-12Si-8.5B (at.%), Intermetallics. 9 (2001): 25-31.

[77] J. Wang, B. Li, R. Li, X. Chen, G.J. Zhang. Bimodal α-Mo grain structure inducing excellent oxidation resistance in Mo-12Si-8.5B alloy at 1100 °C, International Journal of Refractory Metals and Hard Materials. 98 (2021): 105533.

[78] J. Wang, B. Li, S. Ren, R. Li, T. Wang, G.J. Zhang. Enhanced oxidation resistance of Mo-12Si-8.5B alloys with ZrB_2 addition at 1300°C, Journal of Materials Science and Technology. 34 (2018): 635-642.

[79] J. Wang, B. Li, R. Li, X. Chen, T. Wang, G.J. Zhang. Unprecedented oxidation resistance at 900°C of Mo-Si-B composite with addition of ZrB_2, Ceramics International. 46 (2020): 14632-14639.

[80] G.J. Zhang, H. Kou, Q. Dang, G. Liu, J. Sun. Microstructure and oxidation resistance behavior of lanthanum oxide-doped Mo-12Si-8.5B alloys, Int. Journal of Refractory Metals and Hard Materials. 30 (2012): 6-11.

[81] W. Fang, A.D. Shan, X.P. Dong, J.S. Wu. Microstructure and oxidation behavior of directionally solidified Mo-Mo_5SiB_2 (T2)-Mo_3Si alloys, Journal of Alloys and Compounds. 462(1-2) (2008): 436-441.

[82] W. Fang, A.D. Shan, X.P. Dong, J.S. Wu. Oxidation behavior of multiphase Mo_5SiB_2 (T2)-based alloys at high temperatures, Transactions of Nonferrous Metals Society of China. 17(6) (2007): 1242-1247.

[83] W.J. Choi, C.W. Park, J.H. Park, Y.D. Kim, J.M. Byun. Volume and size effects of intermetallic compounds on the high-temperature oxidation behavior of Mo-Si-B alloys, International Journal of Refractory Metals and Hard Materials. 81 (2019): 94-99.

[84] D. Schliephake, A. Kauffmann, X. Cong, C. Gombola, M. Azim, B. Gorr, H.J. Christ, M. Heilmaier. Constitution, oxidation and creep of eutectic and eutectoid Mo-Si-Ti alloys, Intermetallics. 104 (2019): 133-142.

[85] V. Supatarawanich, D.R. Johnson, C.T. Liu. Effects of microstructure on the oxidation behavior of multiphase Mo-Si-B alloys, Materials Science and Engineering A. 344(1-2) (2003): 328-339.

[86] A. Yamauchi, K. Yoshimi, Y. Murakami, K. Kurokawa, S. Hanada. Oxidation behavior of Mo-Si-B in-situ composites, Solid State Phenomena. 127 (2007): 215-220.

[87] I. Rosales, H. Martinez, D. Bahena, J.A. Ruiz, R. Guardian, J. Colin. Oxidation performance of Mo_3Si with Al additions, Corrosion Science. 51(3) (2009): 534-538.

[88] S. Burk, B. Gorr, V.B. Trindade, U. Krupp. Temperature oxidation of mechanically alloyed Mo-Si-B alloys, British Corrosion Journal. 44(3) (2009): 168-175.

[89] S. Burk, H.J. Christ. High-temperature oxidation performance of Mo-Si-B alloys: current results, developments and opportunities, Advanced Materials Research. 278 (2011): 587-592.

[90] P. Jéhanno, M. Böning, H. Kestler, M. Heilmaier, H. Saage, M. Krüger. Molybdenum alloys for high temperature applications in air, Powder Metallurgy. 51(2) (2008): 99-102.

[91] B. Mattuck. High-temperature oxidation III. Zirconium and hafnium diborides, Journal of The Electrochemical Society. 113(9) (1966): 908-914.

[92] J. Cook, A. Khan, E. Lee, R. Mahapatra. Oxidation of $MoSi_2$-based composites, Materials Science and Engineering A. 155(1-2) (1992): 183-198.

[93] Y. Yang, H. Bei, S.L. Chen, E.P. George, J. Tiley, Y.A. Chang. Effects of Ti, Zr, and Hf on the phase stability of Mo_ss + Mo_3Si + Mo_5SiB_2 alloys at 1600°C, Acta Materialia. 58(2) (2010): 541-548.

[94] S. Vorotilo, A.Y. Potanin, Y.S. Pogozhev, E.A. Levashov, N.A. Kochetov, D.Y. Kovalev. Self-propagating high-temperature synthesis of advanced ceramics $MoSi_2$-HfB_2-MoB, Ceramics International. 45(1) (2019): 96-107.

[95] D. Sciti, L. Silvestroni, A. Bellosi. Fabrication and properties of HfB_2-$MoSi_2$ composites produced by hot pressing and spark plasma sintering, Journal of Materials Research. 21(6) (2006): 1460-1466.

[96] A.Y. Potanin, S. Vorotilo, Y.S. Pogozhev, S.I. Rupasov, P.A. Loginov, N.V. Shvyndina, T.A. Sviridova, E.A. Levashov. High-temperature oxidation and plasma torch testing of $MoSi_2$-HfB_2-MoB ceramics with single-level and two-level structure, Corrosion Science. 158 (2019): 108074.

[97] D. Sciti, A. Balbo, A. Bellosi. Oxidation behaviour of a pressureless sintered HfB_2-$MoSi_2$ composite, Journal of the European Ceramic Society. 29(9) (2009): 1809-1815.

[98] T.A. Parthasarathy, R.A. Rapp, M. Opeka, R.J. Kerans. A model for the oxidation of ZrB_2, HfB_2 and TiB_2, Acta Materialia. 55(17) (2007): 5999-6010.

[99] N.K. Kumar, J. Das, R. Mitra. Effect of Zr addition on microstructure, hardness and oxidation behavior of arc-melted and spark plasma sintered multiphase Mo-Si-B alloys, Metallurgical and Materials Transactions A. 50(11) (2019): 2041-2060.

[100] Y. Yu, R. Luo, Q. Xiang, Y. Zhang, T.Y. Wang. Anti-oxidation properties of a BN/SiC/Si_3N_4-ZrO_2-SiO_2

multilayer coating for carbon/carbon composites, Surface and Coatings Technology. 277 (2015): 7-14.

[101] J.H. Choi, Y. Mao, J.P. Chang. Development of hafnium based high-κ materials-A review, Materials Science and Engineering: R. 72(6) (2011): 97-136.

[102] J. Das, R. Mitra, S.K. Roy. Oxidation behaviour of Mo-Si-B-(Al,Ce) ultrafine-eutectic dendrite composites in the temperature range of 500-700°C, Intermetallics. 19(1) (2011): 1-8.

[103] J. Das, B. Roy, N.K. Kumar, R. Mitra. High temperature oxidation response of Al/Ce doped Mo-Si-B composites, Intermetallics. 83 (2017): 101-109.

[104] D.M. Dimiduk, J.H. Perepezko. Mo-Si-B alloys: Developing a revolutionary turbine-engine material, Mrs Bulletin. 28(9) (2003): 639-645.

[105] J.H. Perepezko, R. Sakidja, K.S. Kumar. Mo-Si-B alloys for ultrahigh temperature applications, Advanced Structural Materials. (2006): 437-473.

[106] M.G. Mendiratta, T.A. Parthasarathy, D.M. Dimiduk. Oxidation behavior of αMo-Mo_3Si-Mo_5SiB_2 (T2) three phase system, Intermetallics. 10(3) (2002): 225-232.

[107] C.G. Cofer, J. Economy. Oxidative and hydrolytic stability of boron nitride—A new approach to improving the oxidation resistance of carbonaceous structures, Carbon. 33(4) (1995): 389-395.

[108] T. Karahan, G. Ouyang, P.K. Ray, M.J. Kramer. Oxidation mechanism of W substituted Mo-Si-B alloys, Intermetallics. 87(9) (2017): 38-44.

[109] J. Das, R. Mitra, S.K. Roy. Effect of Ce addition on the oxidation behaviour of Mo-Si-B-Al ultrafine composites at 1100°C, Scripta Materialia. 64(6) (2011): 486-489.

[110] S. Paswan, R. Mitra, S.K. Roy. Isothermal oxidation behaviour of Mo-Si-B and Mo-Si-B-Al alloys in the temperature range of 400-800°C, Materials Science and Engineering: A. 424(1-2) (2006): 251-265.

[111] S. Paswan, R. Mitra, S.K. Roy. Oxidation behaviour of the Mo-Si-B and Mo-Si-B-Al alloys in the temperature range of 700-1300°C, Intermetallics. 15(9) (2007): 1217-1227.

[112] K.K. Cui, Y.Y. Zhang, T. Fu, S. Hussain, T.S. AlGarni, J. Wang, X. Zhang, S. Ali. Effects of Cr_2O_3 content on microstructure and mechanical properties of Al_2O_3 matrix composites, Coatings. 11(2) (2021): 234.

[113] K.K. Cui, Y.Y. Zhang, T. Fu, J. Wang, X. Zhang. Toughening mechanism of mullite matrix composites: A review, Coatings. 10(7) (2020): 672.

[114] S. Paswan, R. Mitra, S.K. Roy. Nonisothermal and cyclic oxidation behavior of Mo-Si-B and Mo-Si-B-Al alloys, Metallurgical and Materials Transactions A. 40 (2009): 2644.

[115] K. Yanagihara, T. Maruyama, K. Nagata. Effect of third elements on the pesting suppression of Mo-Si-X intermetallics (X=Al, Ta, Ti, Zr and Y), Intermetallics. 4(S1) (1996): S133-S139.

[116] D.G. Liu, L. Zheng, L.M. Luo, X. Zan, J.P. Song, Q. Xu, X.Y. Zhu, Y.C. Wu. An overview of oxidation-resistant tungsten alloys for nuclear fusion, Journal of Alloys and Compounds. 765 (2018): 299-312.

[117] Z.Y. Liu, W. Gao, Y.D. He. Modeling of oxidation kinetics of Y-doped Fe-Cr-Al alloys, Oxidation of Metals. 53(3-4) (2000): 341-350.

[118] H. Fujikawa, T. Morimoto, Y. Nishiyama, S.B. Newcomb. The effects of small additions of yttrium on the high-temperature oxidation resistance of a Si-containing austenitic stainless steel, Oxidation of Metals. 59(1-2) (2003): 23-40.

[119] S. Telu, R. Mitra, S.K. Pabi. Effect of Y_2O_3 addition on oxidation behavior of W-Cr alloys, Metallurgical and Materials Transactions A. 46 (2015): 5909-5919.

[120] F.J. Pérez, M.J. Cristóbal, M.P. Hierro, G. Arnau, J. Botella. Corrosion protection of low-nickel austenitic stainless steel by yttrium and erbium-ion implantation against isothermal oxidation, Oxidation of Metals. 54(1-2) (2000): 87-101.

[121] Y. Wu, Y. Umakoshi, X.W. Li, T. Narita. Isothermal oxidation behavior of Ti-50Al alloy with Y additions at 800 and 900°C, Oxidation of Metals. 66(5-6) (2006): 321-348.

[122] S. Majumdar, B. Dönges, B. Gorr, H.J. Christ, D. Schliephake, M. Heilmaier. Mechanisms of oxide scale formation on yttrium-alloyed Mo-Si-B containing fine-grained microstructure, Corrosion Science. 90 (2015): 76-88.

[123] S. Majumdar, D. Schliephake, B. Gorr, H.J. Christ, M. Heilmaier. Effect of yttrium alloying on intermediate to high-temperature oxidation behavior of Mo-Si-B alloys, Metallurgical and Materials Transactions A. 44(5) (2013): 2243-2257.

[124] S. Majumdar, A. Kumar, D. Schliephake, H.J. Christ, X. Jiang, M. Heilmaier. Microstructural and micro-mechanical properties of Mo-Si-B alloyed with Y and La, Materials Science and Engineering A. 573 (2013): 257-263.

[125] E.P. EerNisse. Stress in thermal SiO_2 during growth, Applied Physics Letter. 35(1) (1979): 8-10.

[126] E.A. Irene. Silicon oxidation studies: A revised model for thermal oxidation, Journal of Applied Physics. 54(9) (1983): 5416-5420.

[127] E.J. Opila. Variation of the oxidation rate of SiC in water vapor, Journal of the American Ceramic Society. 82(3) (1999): 625-636.

[128] E.J. Opila, J.L. Smialek, R.C. Robinson, D.S. Fox, N.S. Jacobson. SiC recession caused by SiO_2 scale volatility under combustion conditions: II, thermodynamics and gaseous-diffusion model, Journal of the American Ceramic Society. 82(7) (2004): 1826-1834.

 doi:10.20944/preprints202108.0578.v1

[129] J. Schneider, K. Biswas, G. Rixecker, F. Aldinger. Microstructural changes in liquid-phase-sintered silicon carbide during creep in an oxidizing environment, Journal of the American Ceramic Society. 86(3) (2004): 501-507.

[130] B. Gorr, L. Wang, S. Burk, M. Azim, S. Majumdar, H.J. Christ, D. Mukherji, J. Rösler, D. Schliephake, M. Heilmaier. High-temperature oxidation behavior of Mo-Si-B-based and Co-Re-Cr-based alloys, Intermetallics. 48 (2014): 34-43.

[131] S. Burk, B. Gorr, V.B. Trindade, H.J. Christ. Effect of Zr addition on the high-temperature oxidation behaviour of Mo-Si-B alloys, Oxidation of Metals. 73(1-2) (2010): 163-181.

[132] S. Burk, B. Gorr, H.J. Christ. High temperature oxidation of Mo-Si-B alloys: Effect of low and very low oxygen partial pressures, Acta Materialia. 58(18) (2010): 6154-6165.

[133] M. Asadikiya, P. Foroughi, Y. Zhong, Re-evaluation of the thermodynamic equilibria on the zirconia-rich side of the ZrO_2-$YO_{1.5}$ system, Calphad. 61 (2018): 264-274.

[134] C.S. Du, Q.M. Yuan, Z.F. Yang. Lowering the synthesis temperature of zircon powder by yttria addition, Journal of Materials Science Letters. 18(12) (1999): 965-966.

[135] T. Yang, X.P. Guo. Oxidation behavior of Zr-Y alloyed Mo-Si-B based alloys, International Journal of Refractory Metals and Hard Materials. 88 (2020): 105200.

[136] J.h. You, R.C. Wang, C.B. Liu, X.J. Shi, F. Han, R. Guo, X.W. Liu. Facile synthesis and highly efficient selective adsorption properties of $Y_2Mo_4O_{15}$ for methylene blue: Kinetics, thermodynamics and mechanical analyses, Journal of Rare Earths. 36(8) (2018): 844-850.

[137] N. Takata, N. Sekido, M. Takeyama, J.H. Perepezko, M. Follett-Figueroa, C. Zhang. Solidification of Bcc/T_1/T_2 three-phase microstructure in Mo-Nb-Si-B alloys, Intermetallics. 72(3) (2016): 1-8.

[138] P.K. Ray, M. Akinc, M.J. Kramer. Applications of an extended Miedema's model for ternary alloys, Journal of Alloys and Compounds. 489(2) (2010): 357-361.

[139] J.M. Byun, S.R. Bang, S.H. Kim, W.J. Choi, Y.D. Kim. Mechanical properties of Mo-Nb-Si-B quaternary alloy fabricated by powder metallurgical method, International Journal of Refractory Metals and Hard Materials. 65 (2017): 14-18.

[140] T. Yang, X. Guo. Comparative studies on densification behavior, microstructure, mechanical properties and oxidation resistance of Mo-12Si-10B and Mo_3Si-free Mo-26Nb-12Si-10B alloys, International Journal of Refractory Metals and Hard Materials. 84 (2019): 104993.

[141] V. Behrani, A.J. Thom, M.J. Kramer, M. Akinc. Microstructure and oxidation behavior of Nb-Mo-Si-B alloys, Intermetallics. 14(1) (2006): 24-32.

[142] V. Behrani, A.J. Thom, M.J. Kramer, M. Akinc. Chlorination treatment to improve the oxidation resistance of

 doi:10.20944/preprints202108.0578.v1

Nb-Mo-Si-B alloys, Metallurgical and Materials Transactions A. 36(3) (2005): 609-615.

[143] S. Majumdar. A study on microstructure development and oxidation phenomenon of arc consolidated Mo-Nb-Si-(Y) alloys, International Journal of Refractory Metals and Hard Materials. 78 (2019): 76-84.

[144] L.Y. Udoeva, V.M. Chumarev, A.V. Larionov, S.V. Zhidovinova, S.N. Tyushnyakov. Influence of rare earth elements on the structural-phase state of Mo–Si–X (X = Sc, Y, Nd) in situ composites, Inorganic materials: applied research. 9(2) (2018): 257-263.

[145] B. Roy, J. Das, R. Mitra. Transient stage oxidation behavior of $Mo_{76}Si_{14}B_{10}$ alloy at 1150°C, Corrosion Science. 68 (2013): 231-237.

[146] F.A. Rioult, S.D. Imhoff, R. Sakidia, J.H. Perepezko. Transient oxidation of Mo-Si-B alloys: Effect of the microstructure size scale, Acta Mater. 57(15) (2009): 4600-4613.

[147] T.A. Parthasarathy, M.G. Mendiratta, D.M. Dimiduk. Oxidation mechanisms in Mo-reinforced Mo_5SiB_2 (T2)-Mo_3Si alloys, Acta Materialia. 50(7) (2002): 1857-1868.